VYSOKÉ UČENÍ TECHNICKÉ V BRNĚ
BRNO UNIVERSITY OF TECHNOLOGY

FAKULTA STROJNÍHO INŽENÝRSTVÍ
LETECKÝ ÚSTAV

FACULTY OF MECHANICAL ENGINEERING
INSTITUTE OF AEROSPACE ENGINEERING

INTERLAMINAR FRACTURE TOUGHNESS
OF FIBER REINFORCED PLASTICS
INTERLAMINÁRNÍ LOMOVÁ HOUŽEVNATOST VLÁKNOVÝCH KOMPOZITNÍCH MATERIÁLŮ
S POLYMERNÍ MATRICÍ

DIPLOMOVÁ PRÁCE
MASTER'S THESIS

AUTOR PRÁCE   BC. VÍT VODIČKA
AUTHOR

VEDOUCÍ PRÁCE   DOC. ING. JOSEF KLEMENT, CSC.
SUPERVISOR

BRNO 2014

Vysoké učení technické v Brně, Fakulta strojního inženýrství

Letecký ústav
Akademický rok: 2013/14

ZADÁNÍ DIPLOMOVÉ PRÁCE

student(ka): Bc. Vít Vodička

který/která studuje v **magisterském studijním programu**

obor: **Stavba letadel (2301T039)**

Ředitel ústavu Vám v souladu se zákonem č.111/1998 o vysokých školách a se Studijním a zkušebním řádem VUT v Brně určuje následující téma diplomové práce:

Interlaminární lomová houževnatost vláknových kompozitních materiálů s polymerní matricí

v anglickém jazyce:

Interlaminar fracture toughness of fiber reinforced plastics

Stručná charakteristika problematiky úkolu:

Lomová houževnatost je důležitým parametrem ovlivňujícím chování tzv. damage tolerant konstrukce, tj. konstrukce bezpečně odolávající poškození. U kompozitních materiálů je důležitá interlaminární lomová houževnatost, která je limitována vlastnostmi rozhraní mezi vlákny a polymerní matricí. Vedle složek kompozitního materiálu ovlivňuje tuto charakteristiku výrazně i výrobní technologie. To nezbytně vyžaduje rozsáhlé experimentální ověřování s uvážením konkrétních materiálových a technologických parametrů.

Cíle diplomové práce:

Cílem je získání experimentálních dat interlaminární lomové houževnatosti kompozitních materiálů ve vazbě na projekty řešené na Leteckém ústavu FSI.
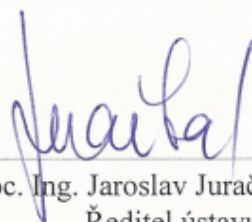
Seznam odborné literatury:

1) ASM Handbook, Vol. 21
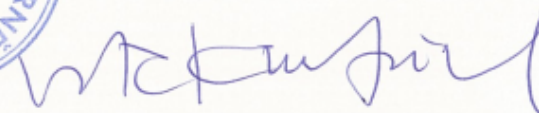2) ASTM D 5528
3) ASTM Z 8320Z
4) ASTM Z 7225Z

Vedoucí diplomové práce:doc. Ing. Josef Klement, CSc.

Termín odevzdání diplomové práce je stanoven časovým plánem akademického roku 2013/14.

V Brně, dne 23.10.2013

L.S.

doc. Ing. Jaroslav Juračka, Ph.D.
Ředitel ústavu

prof. RNDr. Miroslav Doupovec, CSc., dr. h. c.
Děkan

Abstract

The goal of this master`s thesis is to improve understanding of damage tolerance concept by covering all possible effect on fracture toughness of fiber reinforced plastic material. This is achieved by performing test for diverse conditions (e.g. test setups, fracture modes, ply structures and materials) and monitoring its different crack growth behavior. Based on data obtained during these tests, fracture toughness value is determined. Potential discrepancies are discussed and put into context with the rest of specimen.

Keywords

Carbon fiber reinforced plastic, carbon nanotubes, delamination, energy strain release rate, fracture mode, interlaminar fracture toughness

Abstrakt

Cílem této diplomové práce je lépe porozumět konceptu únavového poškození damage tolerance zmapováním všech možných vlivů na lomovou houževnatost vláknového kompozitu s polymerní matricí. Toho je dosaženo provedením zkoušek za různých podmínek (např. změna parametrů měření, mód zatížení, pořadí vrstev a materiál) a monitorováním odlišností v šíření trhliny. Na základě dat získaných během těchto testů je určena lomová houževnatost. Potenciální rozdíly jsou zkonzultovány a porovnány s ostatními vzorky.

Klíčová slova

Uhlíkový vláknový kompozit s polymerní matricí, uhlíkové nanotrubičky, delaminace, hnací síla trhliny, zatěžovací mód, interlaminární lomová houževnatost

Bibliografická citace mé práce

VODIČKA, V. *Interlaminární lomová houževnatost vláknových kompozitních materiálů s polymerní matricí.* Brno: Vysoké učení technické v Brně, Fakulta strojního inženýrství, 2014 75s. Vedoucí diplomové práce doc. Ing. Josef Klement, CSc..

Čestné prohlášení

Prohlašuji, že svou diplomovou práci na téma "Interlaminární lomová houževnatost vláknových kompozitních materiálů s polymerní matricí" jsem vypracoval samostatně pod vedením vedoucího diplomové práce a s použitím odborné literatury, pramenů a dalších informačních zdrojů, které jsou všechny citovány v práci a uvedeny v seznamu literatury na konci práce.

……………………………
Vít Vodička

Acknowledgment

Contents

1. Introduction 12

    1.1   Thesis structure 12

2.   Literature review - theoretical background 13

    2.1   Damage tolerance concept 13

        2.1.1   Safe-life 13

        2.1.2   Damage tolerance 14

    2.2   Fracture mechanics 15

        2.2.1   Fracture modes 15

        2.2.2   Griffith's theory of brittle structure 17

        2.2.3   Irwin`s modification 17

        2.2.4   Energy strain release rate 18

        2.2.5   Stress intensity factor 18

        2.2.6   Fracture toughness 19

    2.3   Fracture in composite materials 19

        2.3.1   Effect of fibers 20

        2.3.2   Fiber bridging 20

        2.3.3   Carbon nanotubes 21

    2.4   Summary 22

3.   Literature review - test procedures 23

    3.1   Mode I – Double cantilever beam – DCB 23

        3.1.1   Mathematical background 23

        3.1.2   Specimen preparation 26

        3.1.3   Testing 27

    3.2   Mode II – End notched flexure – ENF 28

        3.2.1   Mathematical background 28

        3.2.2   Specimen preparation 31

        3.2.3   Test setup 32

4.   Testing 33

    4.1   Mode I - Double cantilever beam, METU 33

        4.1.1   Specimen preparation 33

        4.1.2   Test equipment 35

        4.1.3   Test setup 35

        4.1.4   Experimental output 37

1. Introduction

Composite materials are becoming more and more popular in various fields of the industry. Modern technology brings new problems designers are faced to solve. One of these difficulties is **delamination**. A lot of research to help to understand its mechanism has been done in the last few decades. Even at the moment, scientist round the world still try to improve our knowledge of this phenomenon. Nowadays, most of aerospace designers, follow the **damage tolerance** concept. The complex knowledge of delamination process is fundamental to be able to perform such a design. **Interlaminar fracture toughness** is the material characteristics, which has high impact on under what circumstances delamination occurs. Moreover, it defines if **crack growth** is **stable** or **spontaneous**. Therefore, reliable values are necessary. Such values are obtained by precise material testing process which is the goal of this thesis.

1.1 **Thesis structure**

First part contains brief literature overview of basic terms related to topic. It explains damage tolerance concept and its effect in aerospace engineering. Fundamental terms of fracture mechanics such as fracture toughness and energy strain release rate are defined. Different loading modes are introduced. Basic specifics of fracture in composite material are explained.

Next part describes theoretical background of testing itself. It shows test setups and specimen preparation for each mode and defines its equations.

Main part presents tests performed. It describes loading devices, software and material used in each particular testing. It shows actual difficulties, which occurred during testing and how were they solved.

Analysis is the aim of last part of this thesis. By comparing results obtained under different conditions general conclusions are deduced and presented. It summarizes the contribution and what needs to be improved.

2. Literature review - theoretical background

2.1 Damage tolerance concept

Fatigue damage of aerospace structures can be catastrophic. It has been proved many times in past (e.g. Aloha Airlines - Flight 243, [1]). To prevent such a disasters from happening, investigation reports are made, raising safety issues which must be followed. Based mostly on these safety issues and current available technology level so-called design philosophies are defined. Fundamental two of them are presented.

2.1.1 Safe-life

Fatigue fracture will not develop during the whole service life of the component or the structure - Figure 1, 2.
To be able to fulfil its function, safe – life structures are robust to ensure its reliability throughout the lifetime of the structure. This leads to heavy structure.
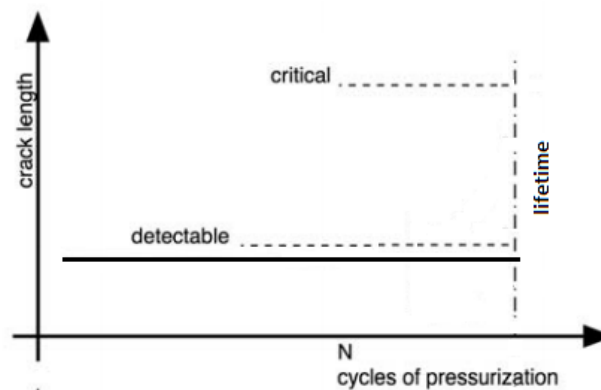
Figure 1: Safe-life, Crack length
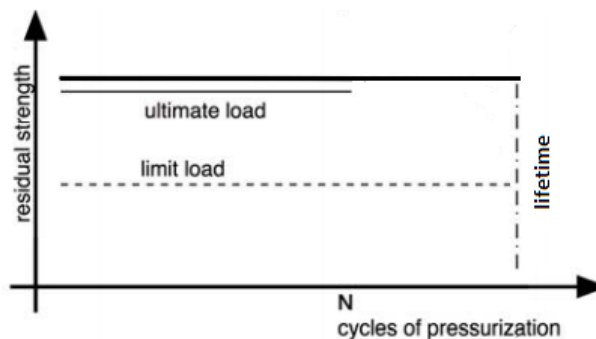
Figure 2: Safe-life, Residual strength

This approach was popular in past, however it is used even nowadays. Mostly in components that cannot be duplicated (e.g. landing gear, beam, etc.). [2, 3]

2.1.2 **Damage tolerance**

Fatigue crack can develop during the service life of the component or the structure. Crack will not reach its critical size before next inspection is performed -.

During inspection crack detection is performed. Areas sensitive to crack initiation such as rivet holes or free edges are inspected carefully. Remaining lifetime of every single crack is calculated. If necessary, damaged components are replaced. Otherwise it can stay until next inspection.

This concept has positive influence on the lifetime of the structure.
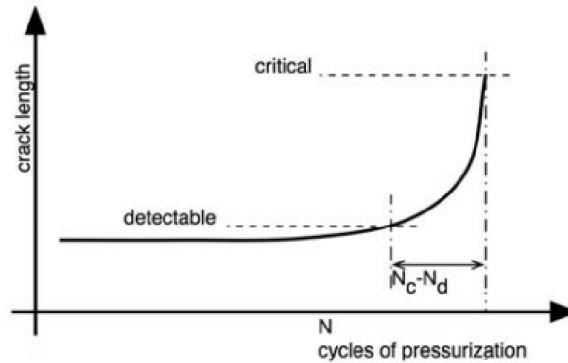
Figure 3: Damage tolerance, Crack length

Figure 3 illustrates inspection interval. To be sure failure does not occur, time between inspections is lesser than time between detectable and critical crack size. Safety factor is applied as well.

$$t_{BI} = (N_c - N_d)/ SF \tag{2-1}$$

Figure 4 shows residual strength remaining.
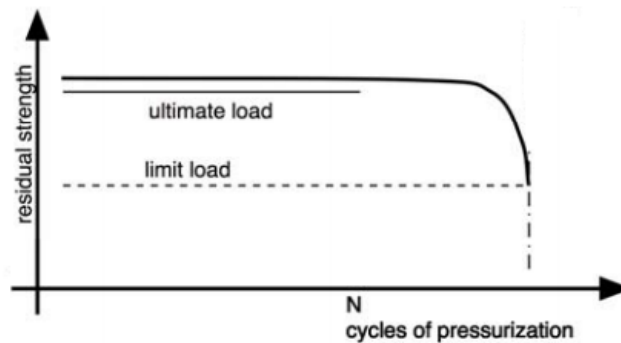
Figure 4: Damage tolerance, Residual strenght

This approach is becoming more and more popular and it is used in components that are subjected to fatigue loading (e.g. fuselage panels, wing panels, etc.).[2, 3]

2.2 **Fracture mechanics**

"Field of study, which describes crack propagation process, using analytical solid mechanics methods".

2.2.1 **Fracture modes**

There are three types of loading, which leads to crack propagation. It is important to note that for each of these modes material shows different fracture characteristics – different value of fracture toughness (e.g. K_{Ic}, K_{IIc}, K_{IIIc})

2.2.1.1 Mode I - Opening

As shown on Figure 5 normal stress is perpendicular to plane of crack.
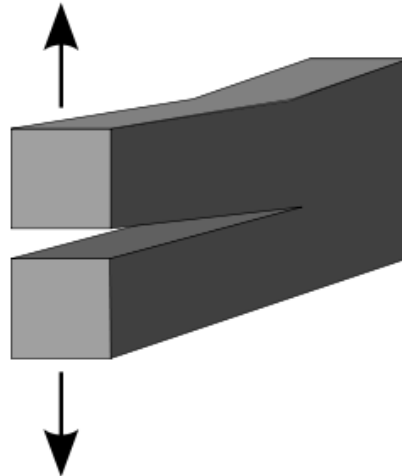
Figure 5: Fracture modes, Mode I – Opening

It is governing mode for the most of metal structures.

Mode I was the aim of the research in last several decades, therefore nowadays it is relatively well understand and there are reliable testing techniques for new materials (e.g. double cantilever beam – DCB).

2.2.1.2 Mode II – Sliding

As shown on Figure 6 shear stress is parallel to crack plane and perpendicular to the crack front.
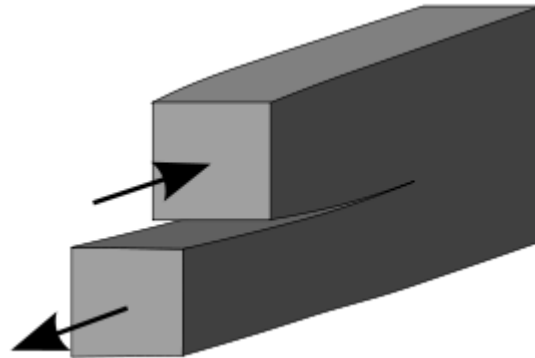
Figure 6: Fracture modes, Mode II – Sliding

Loading mode typical for composite structures (e.g. thermal loading).
Currently, mode II is under intensive research. Since composite structures becoming more popular its importance raises. Nowadays there are several measurement method in use. (e.g. end notched flexure – ENF)

2.2.1.3 Mode III – Tearing

As shown on Figure 7 shear stress is parallel to crack plane and parallel to the crack front.
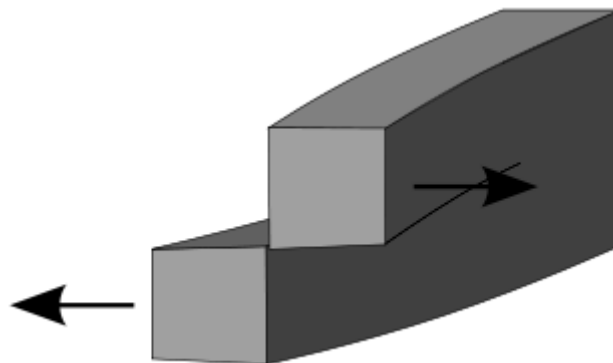
Figure 7: Fracture modes, Mode III – Tearing

Importance of Mode III raised with composite as well and it has increasing effect in today`s design.[4, 5]

2.2.2 Griffith's theory of brittle structure

In 1925 Griffith published his experimental work on cracked glass structures. He observed that square root of crack area A timed the stress at fracture σ_f remains constant.

$$\sigma_f \sqrt{a} \cong C \qquad (2\text{-}2)$$

He claimed that when crack propagates new free crack surface is created. This **surface energy** is higher than in the state before opening. Therefore it is necessary to dissipate some energy for creating this crack surface. Griffith believed this energy is represented by constant in his equation. He found that:

$$C = \sqrt{\frac{2E\gamma}{\pi}} \qquad (2\text{-}3)$$

Where E is the Young's modulus and γ is the surface energy density of the material.
This works well for brittle materials (e.g. glass, ceramics), however for ductile materials (e.g. steel, CFRP) is C usually energy unrealistically high. [4, 5]

2.2.3 Irwin`s modification

Irwin realized there is a **plastic region** in front of the crack - Figure 8. While crack propagates, energy is dissipated to form new plastic regions.
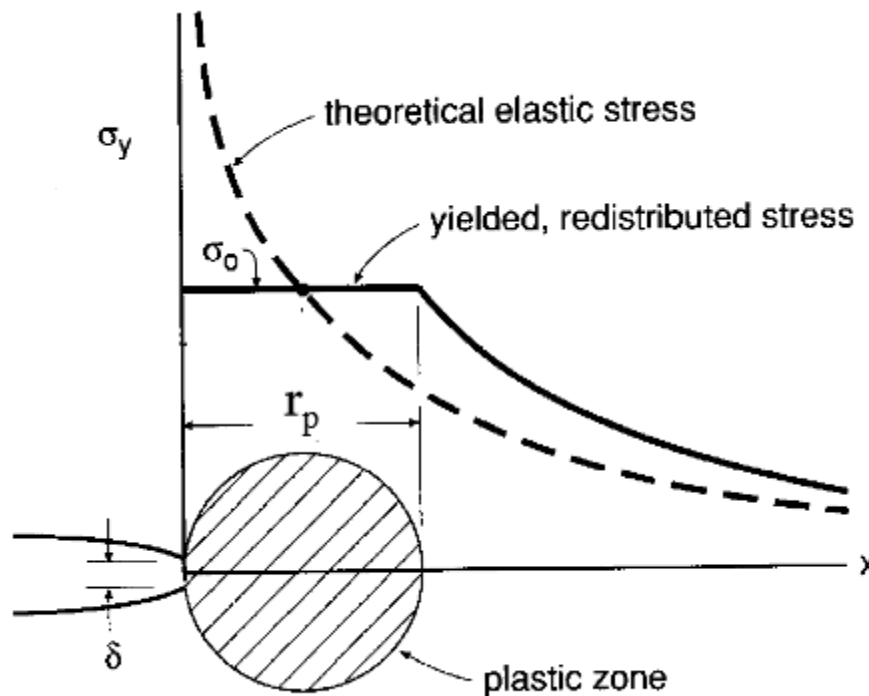
Figure 8: Irwin`s modification, Plastic region zone

He derived its effect on the energy equation:

$$\sigma_f \sqrt{a} = \sqrt{\frac{2\gamma + G_p}{\pi}}$$ (2-4)

Where G_p is the plastic energy dissipation and γ is the surface energy.
For brittle material is G_p negligible therefore Griffith's theory of brittle structure is valid.

It is important to understand that total energy consumed during crack propagation process is sum of surface energy and energy of plastic region.

2.2.4 Energy strain release rate

Energy dissipated during fracture per unit area is defined as **energy strain release rate**.

$$G = -\left[\frac{\partial U}{\partial A}\right]$$ (2-5)

Where U is the elastic energy of the structure and A is area size of the crack.

If the strain energy release rate exceeds a critical value G_c, then crack grows **spontaneously**. It is necessary to avoid this state in damage tolerant design.

2.2.5 Stress intensity factor

So far the problem was described in terms of energy. To define the crack area in term of stress, stress intensity factor is used instead.
Crack tip geometry is illustrated at Figure 9.
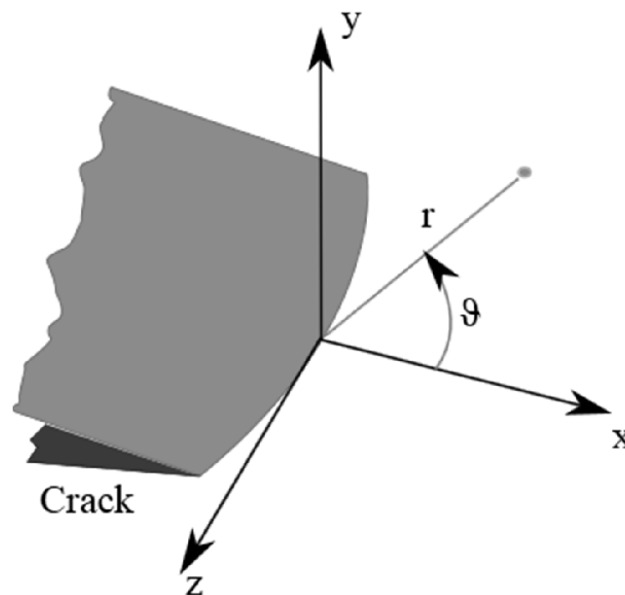
Figure 9: Stress intensity factor, Crack region

Stress field around the crack is defined:

$$\sigma_{ij}(r,\theta) = \frac{K}{\sqrt{2\pi r}} f_{ij}(\theta) + H.O.T.$$

(2-6)

Where σ_{ij} is stress in polar coordinates, K is stress intensity factor and H.O.T. stands for higher order terms which are negligible.

As shown on Figure 8, while r goes close to zero, theoretical elastic stress reaches infinity. In real structure stress decreases due to plastic region round the crack tip defined in last chapter.

If the stress intensity factor exceeds a critical value K_c, then crack will grow **spontaneously**. It describes the same situation as G_c in previous chapter.

K_c is defined as **fracture toughness**. [5, 6]

2.2.6 Fracture toughness

"Fracture toughness is a property which describes the ability of a material containing a crack to resist fracture"[7]

Fracture toughness can be expressed by critical energy release rate.

$$K_c^2 = EG_c$$

(2-7)

It is fundamental value for fracture mechanics. (5)

2.3 Fracture in composite materials

"Composite material is any material made from two or more constituent substances with different chemical and physical properties."

Obviously this definition includes huge variety of materials which are impossible to generalize in terms of fracture mechanics. Therefore this thesis focus on one specific sort of composite materials popular in aerospace design – **Fiber reinforced plastic - FRP**.

FRP consist of brittle continuous fibers and ductile usually epoxy resin plastic.

2.3.1 Effect of fibers

Generally, when crack tip reaches the fiber, it cannot continue through the fiber, but it bypasses it instead. This lead to longer crack path and more energy is consumed. That means the fracture toughness is higher than in case of pure resin.
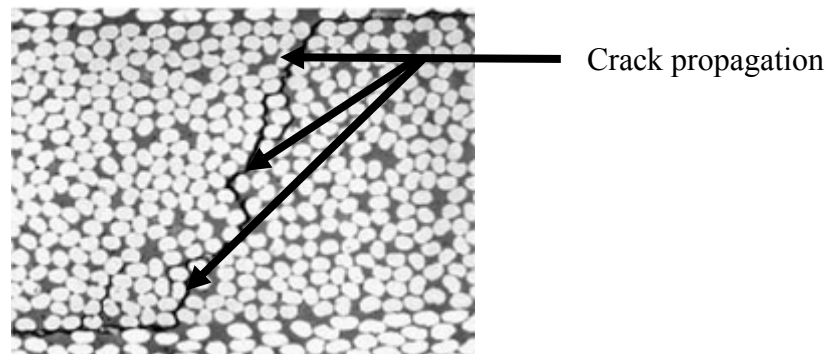
Figure 10: Effect of fibers, crack propagation line

Figure 10 shows that crack follows boundaries of resin and fibers. **Fiber/matrix interface strength** has major effect on its mechanical properties, therefore proper surface treatment is necessary. [8, 9]

2.3.2 Fiber bridging

Fiber bridging mechanism is illustrated on Figure 11.
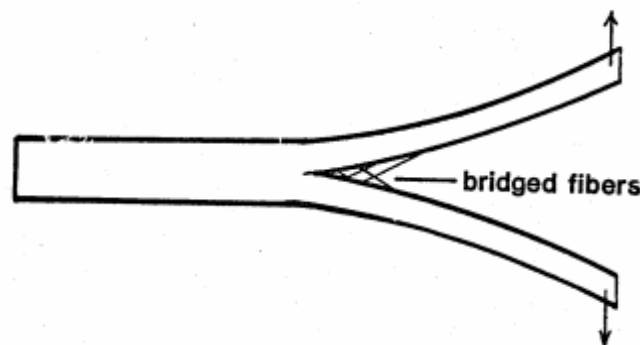
Figure 11: Fiber bridging, Fiber bridging mechanism

The bridged fibers prevents crack from growing, therefore higher load needs to be applied.
This is desirable mechanism in design of the real structure. On the other hand this can lead to misleading values of fracture toughness during testing. Energy consumed by deboning bridged fibers can reach up to 60% of the total energy spend during the crack propagation. Therefore this mechanism has to be taken into account and tested specimen shall be inspected.
Fiber bridging often occurs in mode I testing of unidirectional roving specimen. [10]

2.3.3 **Carbon nanotubes**

Part of this thesis investigates the effect of nanotubes dispersed in composite resin, therefore basic theoretical introduction is presented for this specific topic.

Carbon nanotubes are molecular scale graphitic carbon tubes with extraordinary thermal, electrical and mechanical properties.

In terms of structure there are two types of CNTs - Figure 12. **Single-walled nanotubes – SWNT** are produced by laser evaporation and have excellent mechanical properties – (E ~ 1 TPa, Rm ~ 30 GPa).

On the other hand there are **multi-walled nanotubes – MWNT**. Its mechanical properties does not reach such high values as SWNT, however its manufacturing technology - chemical vapor deposition out of carbon oxygen, is much more productive and therefore more useful for practical application.
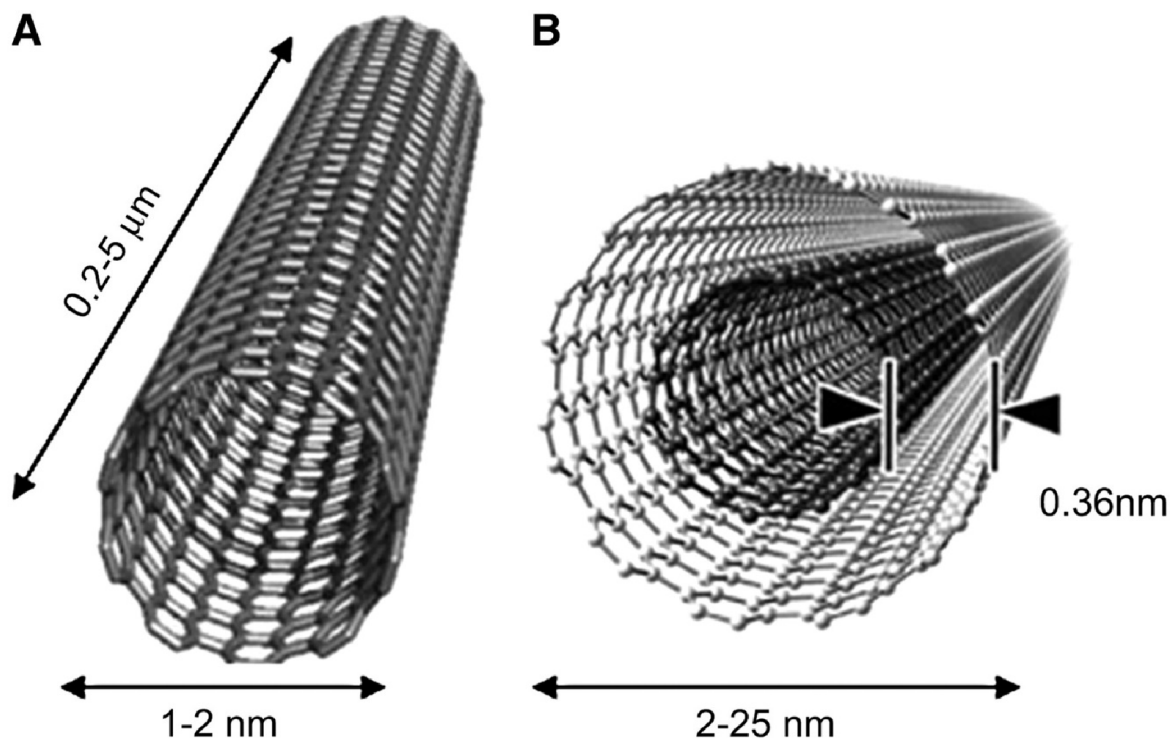
Figure 12: CNT, A – Single walled nanotubes, B – Multi walled nanotubes [11]

CNTs affects fracture mechanics properties in several ways. First, evenly dispersed they enhance fibber bridging mechanism. Real structure example is shown at Figure 13
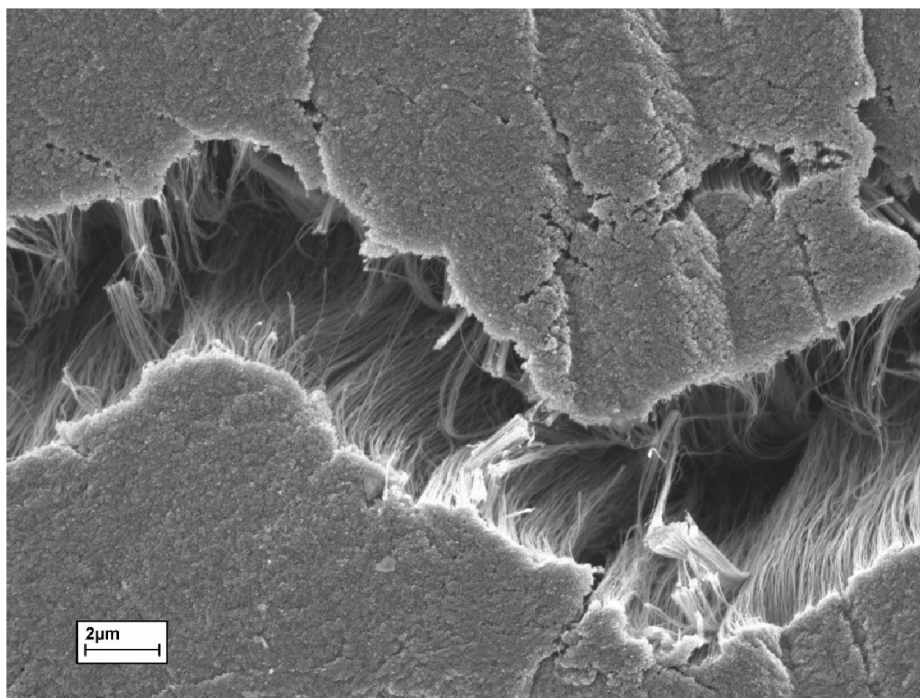
Figure 13: CNT, Fiber bridging [12]

Next CNTs help to block crack as it growths, which leads to higher amount of energy spent - Figure 14.
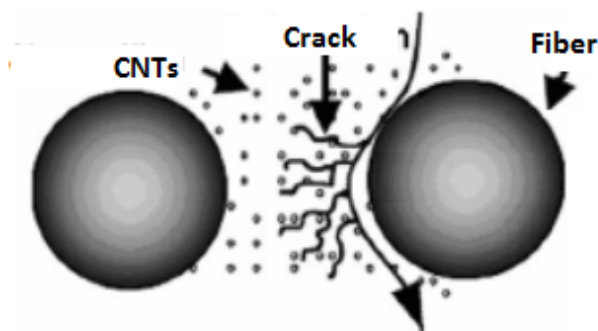
Figure 14: CNT, crack growth hindering [13]

Due to these facts, manufacturing technology of resin dispersed CNTs is nowadays under intensive research to help to improve fatigue properties of composite materials.

Generally, fatigue properties of composite materials are considered as one of its main advantages.

2.4 Summary

The goal of the tests performed in this thesis is to obtain precise reliable values of the fracture toughness of CFRP for different loading modes, material composition and manufacturing process.

3. Literature review - test procedures

In this chapter, there are the most common test methods to obtain fracture toughness of CFRP for different loading modes presented.

3.1 Mode I – Double cantilever beam – DCB

This method was standardized in ASTM D5528. [14]

3.1.1 Mathematical background

Nowadays, there are several ways how to calculate mode I interlaminar fracture toughness G_{IC} – Beam theory (BT), Modified beam theory (MBT), Compliance calibration (CC) and Modified compliance calibration (MCC). Beam theory gives inaccurate data. However it defines the basic approach for the other methods. Generally, G_{IC} data values of MBT, CC and MCC do not differ more than 5%.

3.1.1.1 Beam theory

Uncracked portion of DCB specimen is considered as rigid support for pair of cantilever beams formed by crack.
DCB test is performed on loading machine with fixed displacement. When critical value of displacement is reached crack propagates. Specimen is not able to transmit such a load anymore which leads to force drop. This load difference is proportional to change in strain energy, which can be calculated as area between loading curves. [14]
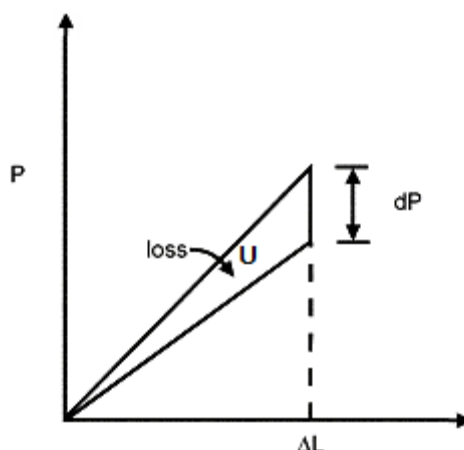
Figure 15: DCB, Load-displacement curve – fixed displacement

Theoretically it is possible to perform test with fixed force as well, but due to its practical difficulties, it is not as common as fixed displacement ones.
To determine critical strain energy release rate, Equation (2-5) is used.

$$G_{IC} = -\left[\frac{\partial U}{\partial A}\right]$$

(3-1)

It is supposed the width **b** is constant. Strain energy is defined in form of loading force and specimen compliance:

$$G_{IC} = \frac{P^2}{2b}\left(\frac{dC}{da}\right) \tag{3-2}$$

Compliance of DCB specimen is defined as:

$$C = \frac{8a^3}{Ebh^3} \tag{3-3}$$

Beam theory defines G_{IC} as:

$$G_{IC} = \frac{3P\delta}{2ba} \tag{3-4}$$

3.1.1.2 Modified beam theory

Previous relation considers beam perfectly build-in. As shown on Figure 16 in real situation there is rotation on delamination front which can`t be neglected. Correction factor has to be applied.
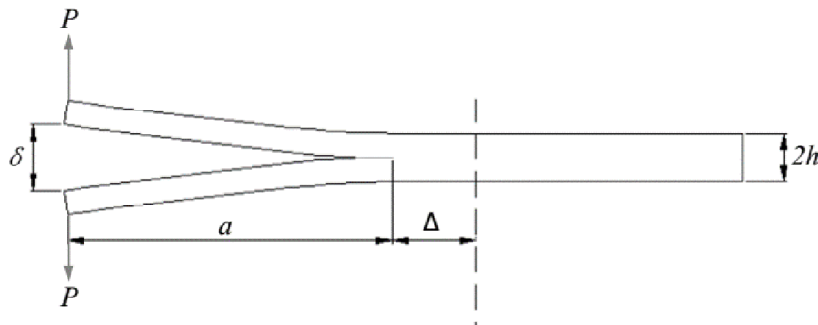
Figure 16: Modified beam theory DCB specimen

This method assumes that the cracked part of the specimen consisting of an upper arm and lower arm can be represented as two cantilever beams built-in at distance Δ in front of the crack tip.
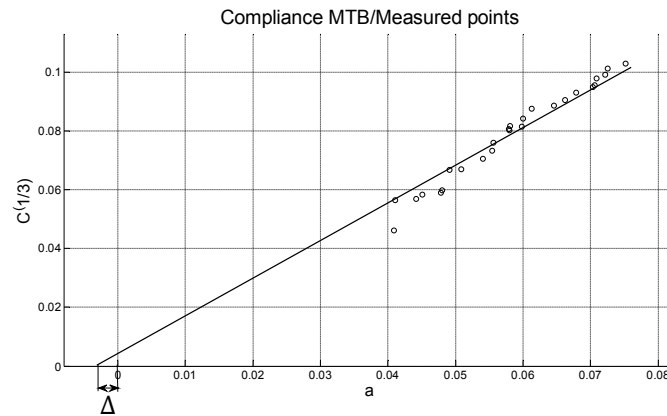
Figure 17: MBT correction line

Corrected formula is then defined as following [15]:

$$G_{IC} = \frac{3P\delta}{2b(a - \Delta)}$$

(3-5)

3.1.1.3   Compliance calibration

Compliance can be defined as:

$$C = Ra^n$$

(3-6)

Where **R** describes geometrical and material properties of the specimen.
This method modifies G_{IC} using linear trend line of compliance and crack length measured data in logarithmic scale. From that trend line it optimizes correction factor n = Δy/Δx as shown:
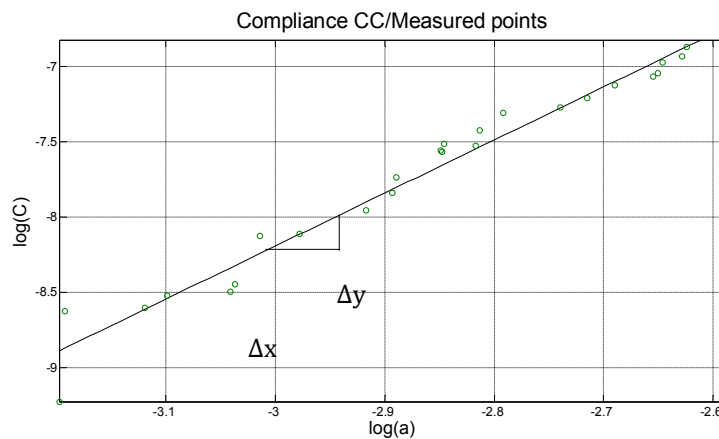

Figure 18: Compliance calibration correction line

Formula is then defined as following [14]:

$$G_{IC} = \frac{nP\delta}{2ba}$$

(3-7)

3.1.1.4   Modified compliance calibration

This method defines normalized compliance as:

$$C = \frac{8a^3}{Ebh^3} \rightarrow \frac{a}{h} = \alpha_1 C^{\frac{1}{3}} + \alpha_0 \qquad (3\text{-}8)$$

This method obtains G_{IC} using linear trend line of measured data of $C^{1/3}$ and a/h. From that trend line it defines correction factor $\alpha 1$ as a slope of this line as shown:
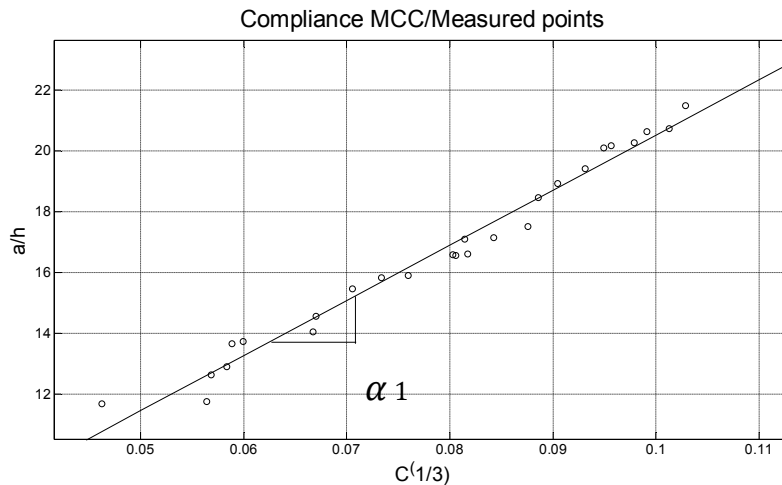
Figure 19: MCC correction line

Formula is then defined as following [14]:

$$G_{IC} = \frac{3P^2 C^{2/3}}{2\alpha_1 bh} \qquad (3\text{-}9)$$

ASTM standards presents all these methods to determine G_{IC} to help to avoid potential error during calculation.

3.1.2   **Specimen preparation**

DCB specimen contains initial crack created by inserting Teflon ply to the midplane of the specimen during its manufacturing. To transmit load from loading device to specimen piano hinges are glued on the end of the specimen. On Figure 20 specimen ready to testing is illustrated.
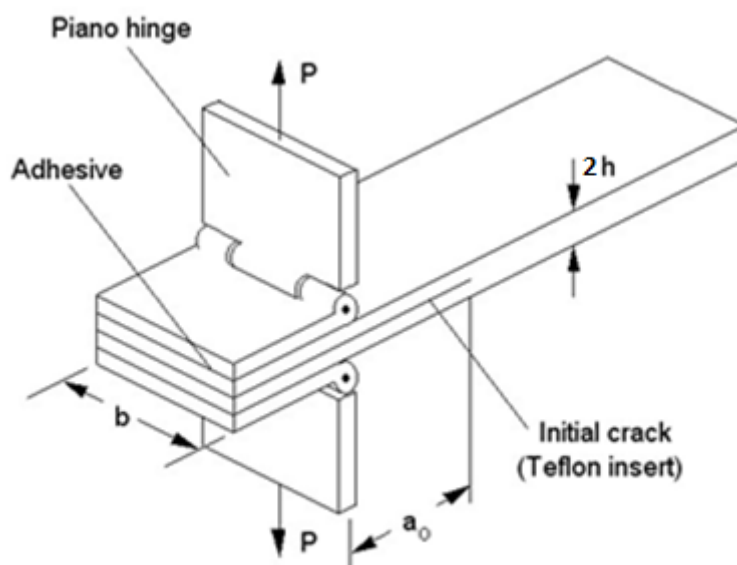
Figure 20: DCB, Experimental setup

3.1.3 Testing

First, the length **L**, width **b** and thickness two **h** of the specimen is measured. The specimen is put into loading device and it is calibrated. It is important that specimen is in horizontal position so the loading line is perpendicular to the crack propagation direction - Figure 21. Load is applied using loading speed up to 5 mm/min. When the initial crack length is readable, loading is paused and the initial crack length a_0 is measured, then continue test. When the crack starts to propagate, write down force **P** and displacement **δ** values and measure the actual crack length **a**.
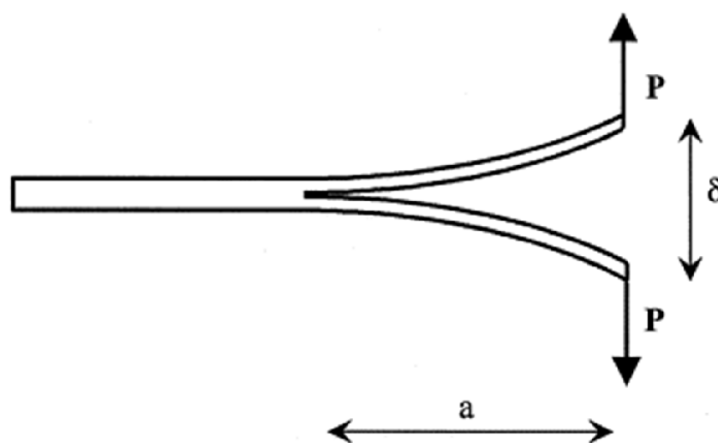
Figure 21: DCB, Scheme of the test

The process is repeated several times whenever cracks propagate. The common way how to measure crack length is by high resolution camera. Whole process can be automatized using photo recording device. At the end of procedure unload the specimen. [14]

3.2 Mode II – End notched flexure – ENF

There are no official standards for this method, therefore tests were performed as advised in literature. [16]

3.2.1 Mathematical background

To calculate G_{IIC}, again it is necessary to determine compliance of ENF specimen:
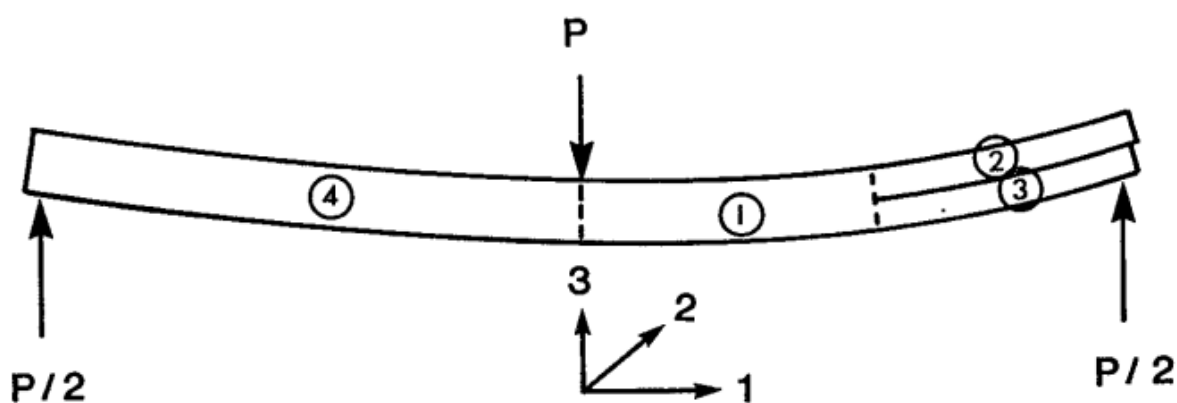

Figure 22: ENF, Specimen regions

As shown on Figure 22, 23 specimen is divided into 4 regions. Coordinate system origin is placed into a loading point of upper support.
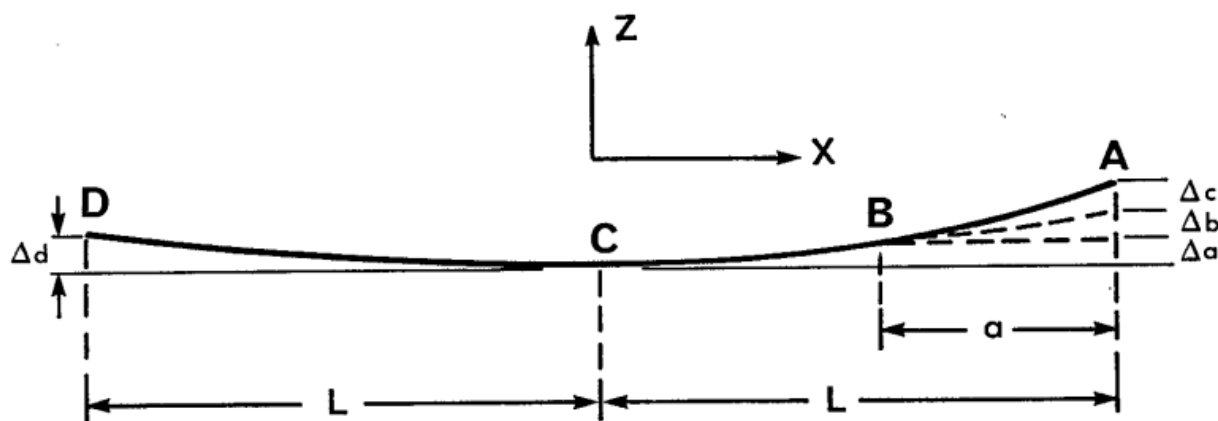

Figure 23: ENF, Specimen deformation

Crack including half of the specimen deflection can be defined as a sum of three partial deflections:
Δa - displacement due to curvature in AB, **Δb** - displacement due to slope at B, **Δc** - displacement due to curvature in BC, **Δd** is the displacement of the solid half.
Displacement due to curvature in AB Δa:

$$\Delta a = \int_0^{L-a} k_1^{(1)} \, dx \tag{3-10}$$

Curvature definition:

$$k_1^{(1)} = d_{11}^{(1)} M_1^{(1)} = \int_0^x d_{11}^{(1)} \frac{P(L-x)}{2b} \, dx \tag{3-11}$$

$$\Delta a = \frac{d_{11}^{(1)}}{12b} P(2L^3 - 3aL^2 + a^3) \tag{3-12}$$

$d_{11}^{(1)}$ is bending – twisting matrix coefficient.
Displacement due to slope at B Δb:

$$\Delta b = a \frac{dz}{dx} = a \int_0^{L-a} \frac{d_{11}^{(1)}}{2b} P(L-x) dx \tag{3-13}$$

$$\Delta b = \frac{d_{11}^{(1)}}{4b} P(aL^2 - a^3) \tag{3-14}$$

Displacement due to curvature in BC Δc:
For every symmetric midplane crack insert specimen:

$$d_{11}^{(2)} = d_{11}^{(3)} \tag{3-15}$$

$$\Delta c^{(2)} = \Delta c^{(3)} = \int_{L-a}^{L} \int_0^x d_{11}^{(2)} \frac{P(L-x)}{2b} \, dx \, dx \tag{3-16}$$

$$\Delta c = \frac{P}{12b} (a^3) d_{11}^{(2)} \tag{3-17}$$

Total deflection at cracked half of specimen Δ:

$$\Delta = \Delta a + \Delta b + \Delta c = \frac{P}{6b}(L^3 - a^3)d_{11}^{(1)} + \frac{P}{12b}(a^3)d_{11}^{(2)} \tag{3-18}$$

For unidirectional midplane crack insert specimen:

$$d_{11}^{(2)} = d_{11}^{(3)} = 8d_{11}^{(1)} \tag{3-19}$$

$$\Delta = \frac{P}{6b}(L^3 - 3a^3)d_{11}^{(1)} \tag{3-20}$$

Displacement of uncracked part Δd:
Substituting a=0 we obtain deflection of uncracked part:

$$\Delta d = \frac{P}{6b}L^3 d_{11}^{(1)} \tag{3-21}$$

From deflections of the end points we can easily determine displacement in the middle - Figure 24.
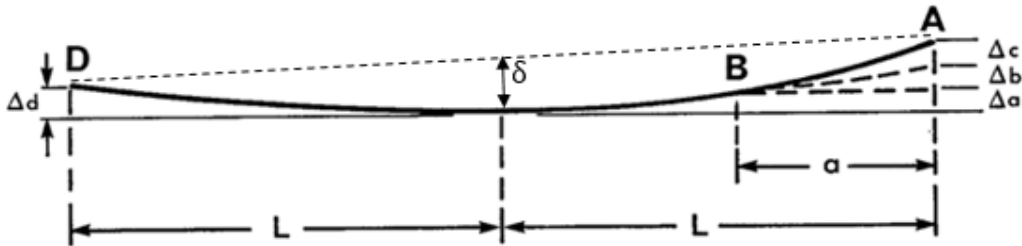
Figure 24: ENF, Middle point specimen deformation

$$\delta = \frac{\Delta a + \Delta b + \Delta c + \Delta d}{2} = \frac{P}{12b}(2L^3 - 3a^3)d_{11}^{(1)} \tag{3-22}$$

Substituting $d_{11}^{(1)}$:

$$\delta = \frac{P}{8bh^3 E}(2L^3 - 3a^3) \tag{3-23}$$

Compliance of ENF specimen:

$$C = \frac{\delta}{P} = \frac{(2L^3 - 3a^3)}{8bh^3 E} \tag{3-24}$$

Interlaminar fracture toughness is related to the compliance by:

$$G = \frac{P^2}{2b}\left(\frac{dC}{da}\right)$$

(3-25)

Then combining get G_{IIC} as:

$$G_{IIC} = \frac{9P^2a^2}{16b^2h^3E}$$

(3-26)

Substituting P= δ/C:

$$G_{IIC} = \frac{9P\delta a^2}{2b(2L^3 + 3a^3)}$$

(3-27)

3.2.2 Specimen preparation

Test is performed on ENF specimen. It contains initial crack created by inserting Teflon ply to the midplane of specimen during its manufacturing. To obtain stable crack growth during test, the initial crack length a_0 shall meet following requirements:

$$0.6 < a_0/L < 1$$

(3-28)

Specimen dimensions are illustrated on Figure 25.
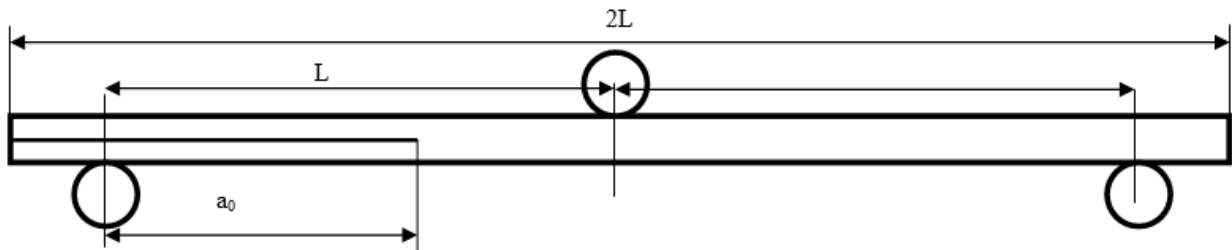
Figure 25: ENF, Specimen sketch

3.2.3 **Test setup**

Again specimen`s dimensions are measured and it is put into loading device - Figure 26. Specimen is loaded at up to 3 mm/min loading speed - critical displacement is lower compare to DCB test.
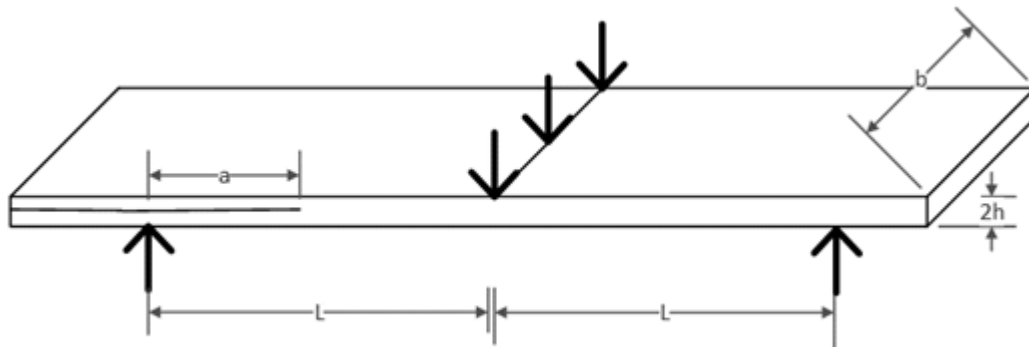

Figure 26: ENF, Experimental setup [8, 17]

When crack propagates photos are taken. Again whole process can be automatized using photo recording device. When crack reaches the middle point of specimen test is stopped.

4. Testing

Experimental testing were partly performed during summer school in Middle East Technical University - **METU**, Ankara, Turkey supervising by Assoc.Prof.Dr. Demirkan Çöker and partly in Brno University of Technology – **BUT** supervising by doc. Ing. Josef Klement, CSc.

The main goal of METU tests was to inspect the effect of **carbon nanotubes - CNTs** distributed in the epoxy resin on interlaminar fracture toughness. Verify the technology of implementing them into resin and find the proper treatment for uniform dispersion.
Moreover **ply orientation effect** was inspected on several specimens. Particularly difference between unidirectional roving and 0/90 fabric.
Mode I and mode II tests were accomplished for specimen with and without CNTs there in METU.

Tests performed in BUT aimed to describe the effect of different composite **fiber mass ratio** on interlaminar fracture toughness. Since BUT specimens were manufactured by another technology than these in METU both of them were discussed and compared.
Mode II and mixed mode tests there were accomplished there in BUT.

4.1 Mode I - Double cantilever beam, METU

To examine effect of CNTs in CFRP for mode I DCB tests were performed.

4.1.1 Specimen preparation

To inspect CNTs effect two specimen with and two without them were manufactured.

4.1.1.1 Material

Specimens were made from HexPly 8552 epoxy matrix prepreg which is regularly used for primary aerospace structures design. Its properties are defined on.

Half of them contains unidirectional - $[0°]_{16}$ with following physical properties:

Table 1: Material properties – METU, Prepreg – HexPly 8552 UD carbon prepregs [18]

Physical properties	Units	AS4
Fiber density	g/cm³	1.79
Filament count/tow		12K
Resin density	g/cm³	1.30
Nominal cured ply thickness	mm	0.130
Nominal fiber volume	%	57.42
Nominal laminate density	g/cm³	1.58

The rest contains cross ply - $[0°/90°]_8$ fibers.

Table 2: Material properties – METU, Prepreg – HexPly 8552 Woven carbon prepregs [18]

Physical properties	Units	AGP 280-5H
Fiber type		AS4 3K
Fiber density	g/cm^3	1.77
Weave		5HS
Mass	g/m^2	286
Weight ratio, Warp: Fill		50:50
Nominal cured ply thickness	mm	0.289
Nominal fiber volume	%	55.29
Nominal laminate density	g/cm^3	1.57

Both kind of specimen contains the same number of plies, but CNTs plies are thicker that non – CNTs one, therefore different thickness for each kind of specimen were obtained.

4.1.1.2   CNT treatment

For CNTs specimen specific approach was used. First CNTs were treated in **methanol bath**. Then they were milled by steel balls to separate its clustered regions. Then **ultra-sonication** was performed to achieve **required dispersion** of milled nanotubes. At the end, CNTs were separated from the liquid by methanol vaporization. Obtained CNTs were then evenly distributed on carbon/epoxy plies. [19]

Non - CNTs specimens were prepared exactly as described in section 3.1.2.

4.1.1.3   Manufacture

Specimens were manufactured from **prepreg – vacuum bag** technology - Figure 27.
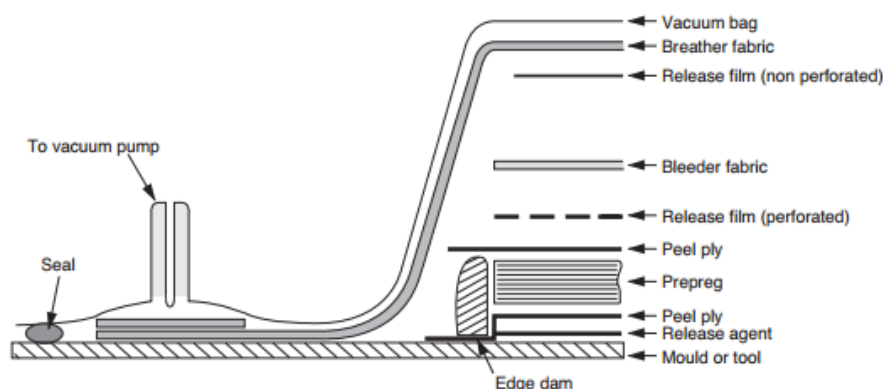

Figure 27: Specimen preparation – METU, prepreg – vacuum bag technology [19]

Then it was cured in **autoclave** using following curing cycle recommended by material producer. Curing cycle is visualized on Figure 28.

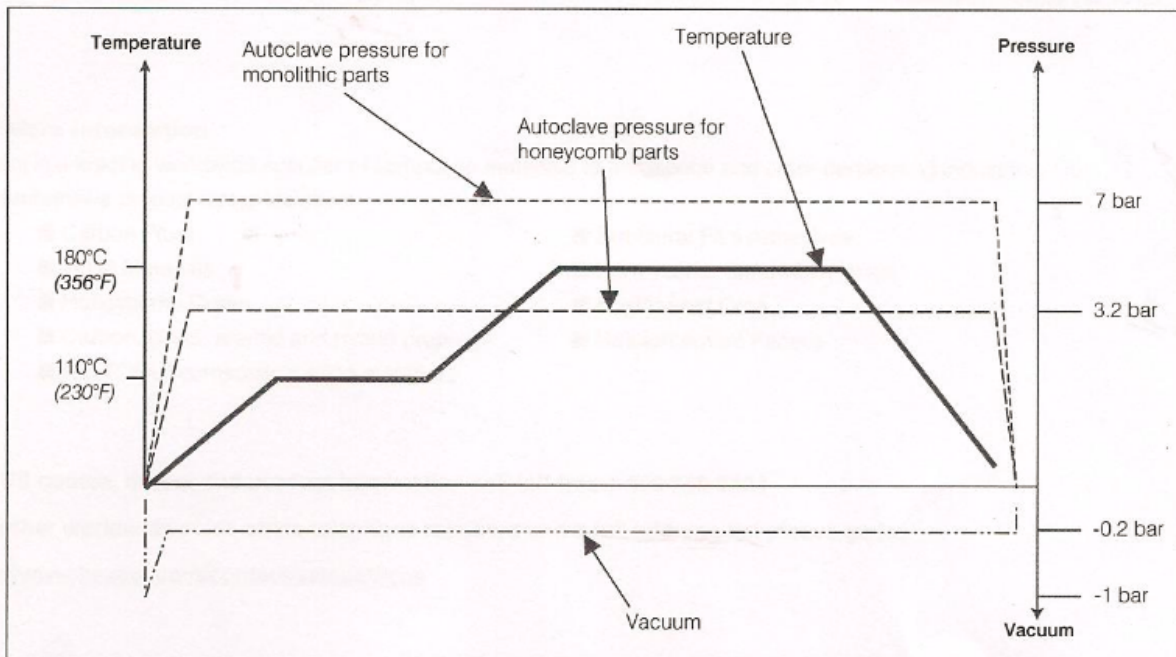**Curing Cycle for Honeycomb and Monolithic Components**

Figure 28: Specimen preparation – METU, curing cycle [20]

After curing, single specimens were cut according ASTM D5528 standard. [14]
Specimen preparation process was performed in Turkish Aerospace Industry – TAI facilities.

Unfortunately, on the first sight manufactured CNTs unidirectional specimens showed poor material quality (e.g. voids, rough surface) which could significantly influence the experimental results.

4.1.2 Test equipment

Tests were performed on AG-IS Autograph universal testing instrument produced by Shimadzu company. Sampling frequency was 20 Hz.
This machine communicated with TRAPEZIUM 2 software installed on the computer. [21] Experimental data were exported into Microsoft excel database and then post processed in Matlab software. Closer look at data processing is in chapter 5.
Database and script files are in the appendix of this thesis.

4.1.3 Test setup

Tests were performed as described in section 3.1.3.
To see crack easier side of specimen was paint white. Moreover scale paper was attached to specimen to read length directly from photos.
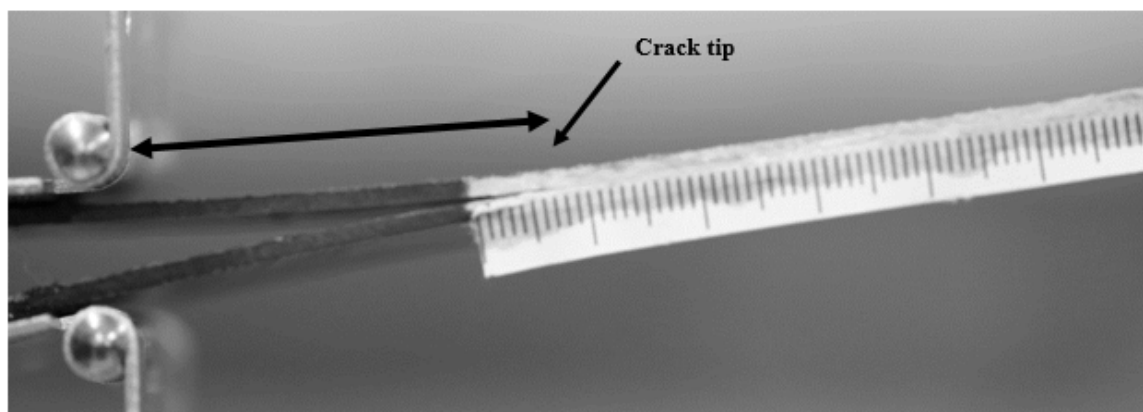
Figure 29: DCB, nonCNTs specimen, initial crack length

The same procedure was performed for specimens with dispersed CNTs.

Figure 30: DCB, CNTs specimen (poor material quality), initial crack length

When sufficient amount of experimental data was obtained test was stopped.
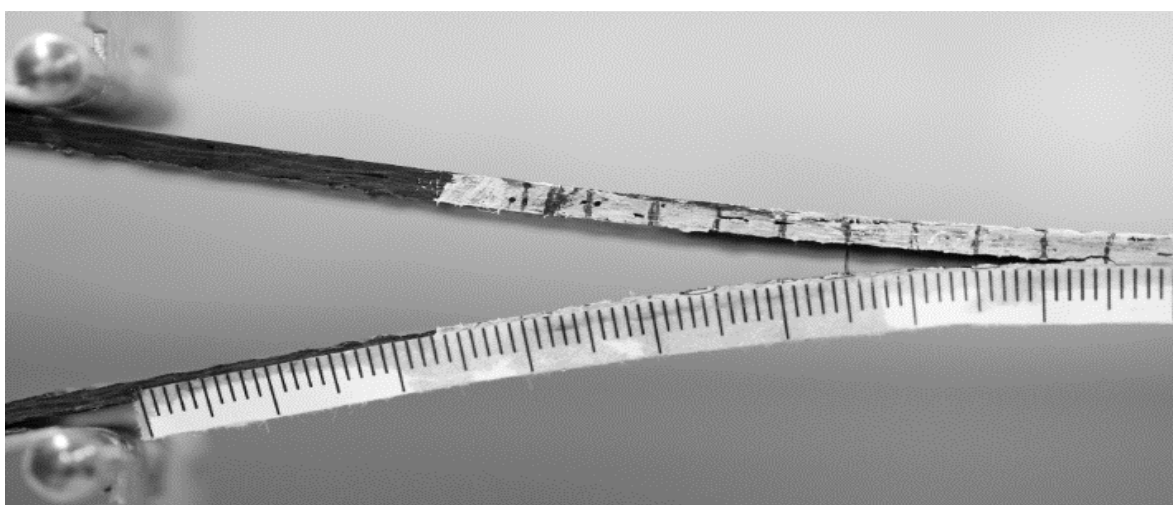

Figure 31: DCB, CNTs specimen (poor material quality), end crack length

4.1.4 **Experimental output**

During testing TRAPEZIUM 2 software record the force and the displacement in loading machine clamps – drawing **load displacement curve**.

4.1.4.1 Load displacement curve

Sloped parts of curve represents load test with no change in specimen structure. On the other hand vertical load drops represents crack growth phase, therefore it is necessary to take photo before these drops occurs.
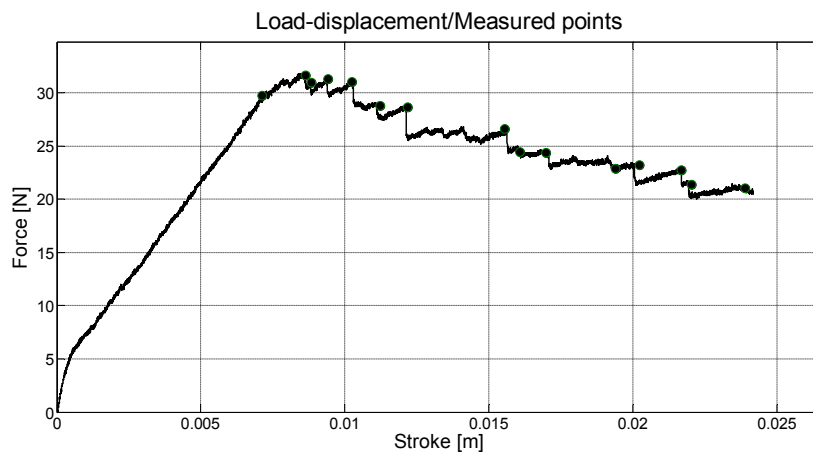

Figure 32: DCB, Load displacement curve

Tips of the curve, shows the maximum load which structure can transmit just before crack progress. That is why these data are fundamental for fracture toughness definition.

4.1.4.2 Resistance curve

Resistance curve shows how fracture toughness changes with crack length. Tendency of resistance curve (trend line) is important.
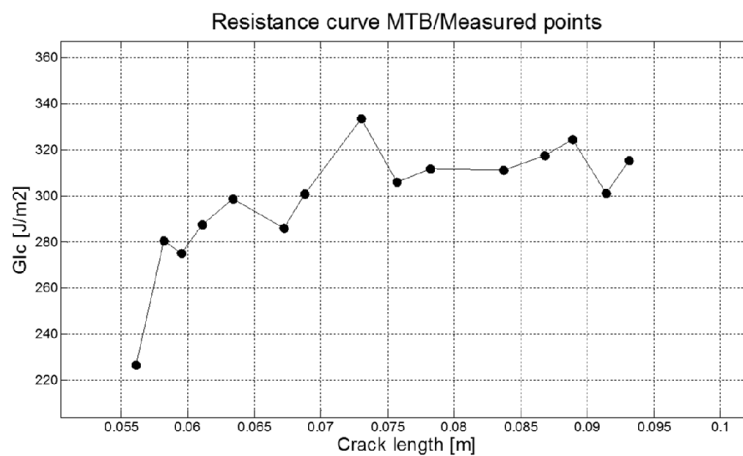

Figure 33: DCB, Resistance curve

The initial point can be affected by manufacturing process therefore it differs from the others.

4.2 Mode II - End notched flexure, METU

To examine effect of CNTs in CFRP for mode II ENF tests were performed.

4.2.1 Specimen preparation

To achieve the same thickness of specimen, different number of plies were used on different kind of specimen. That is because CNTs ply thickness is 0.35 mm and non-CNTs is 0.25 mm. To keep specimen thickness 3 mm, CNTs consist of 8 plies and non- CNTs of 12 plies.

Four specimens were prepared as described in section 3.2.2.

The same technology of CNTs treatment and dispersion as in DCB case was used.

Since there are no ASTM standards for ENF testing, specimen were cut in the same shape as advised in literature. [16]

4.2.2 Test equipment

Test was performed on the loading machine AG-IS and using the software TRAPEZIUM 2, same as in DCB case.

4.2.3 Test setup

Tests were performed as described in section 3.2.3.

Again, face of specimen was painted white and paper scale was attached.
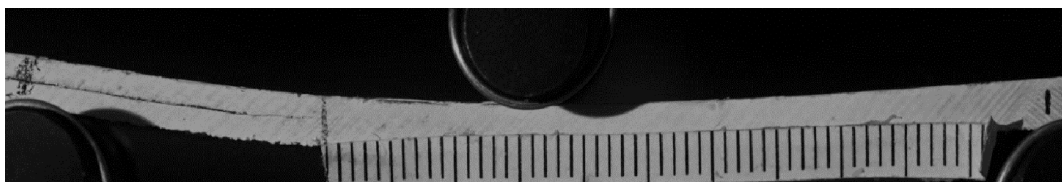

Figure 34: ENF, Test setup
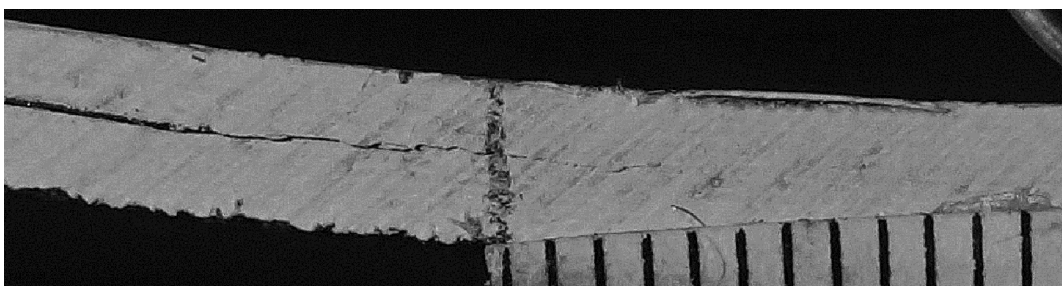
When visible, crack tip was marked.

Figure 35: ENF, Initial crack length

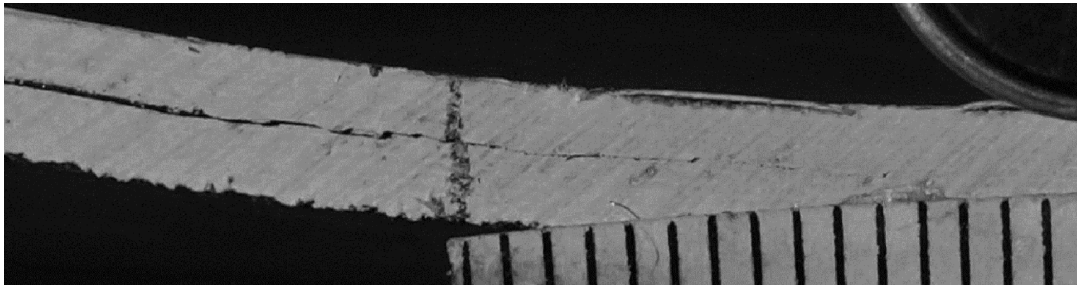For each crack growth photo was taken and crack length is measured.

Figure 36: ENF, End crack length

When crack tip reaches area close to the middle loading point (specified in section 3.2.2) test is stopped.

4.2.3.1   X-ray validation

To confirm the validity of results, crack length obtained by reading photos were compared to crack length obtained from x-ray image of the specimens - Figure 37.
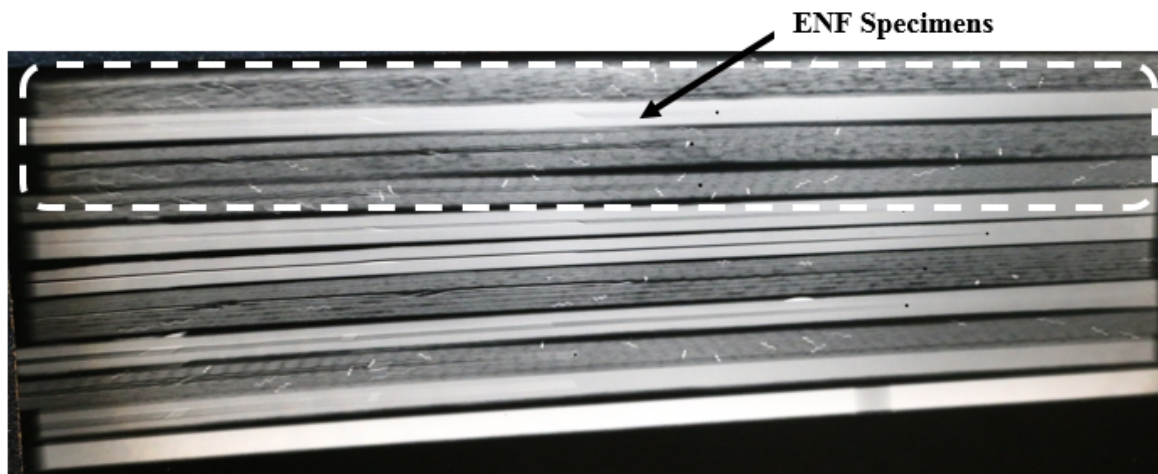

Figure 37: ENF, X-ray validation

The crack lengths obtained from x - ray matched the photos accurately, however half of them were not even readable, therefore it doesn`t seem to be reliable form of data validation.

4.2.4   Experimental output

4.2.4.1   Load displacement curve

Compare to DCB test load drops are not so obvious in ENF. Practically it was more complicated to catch the moment when crack progress. Therefore lesser measuring points were obtained.
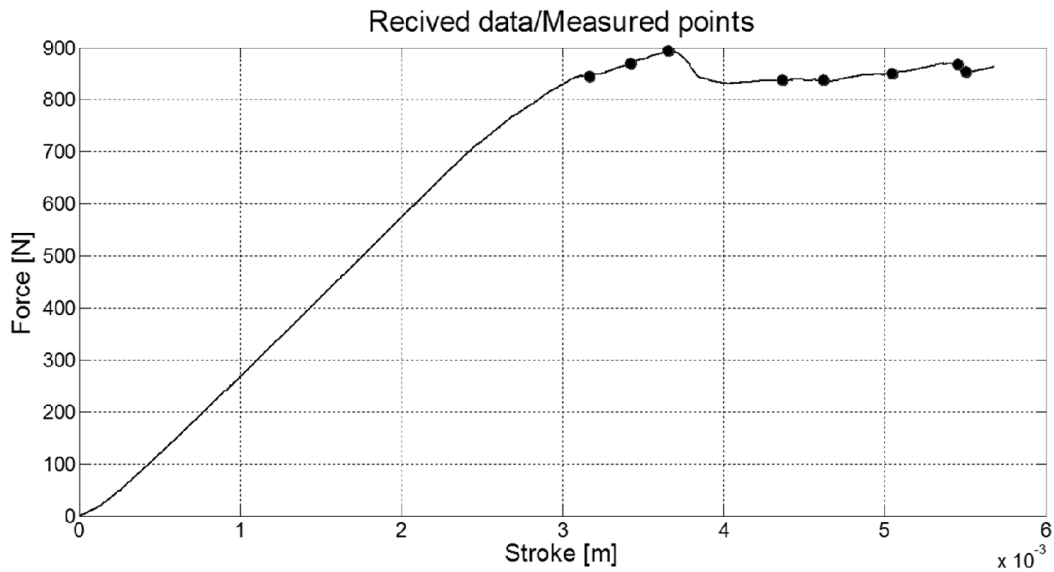
Figure 38: ENF - METU, Load displacement curve

4.2.4.2   Resistance curve

Since there is not so much space for crack propagation in ENF, resistance curve covers smaller length compare to DCB.
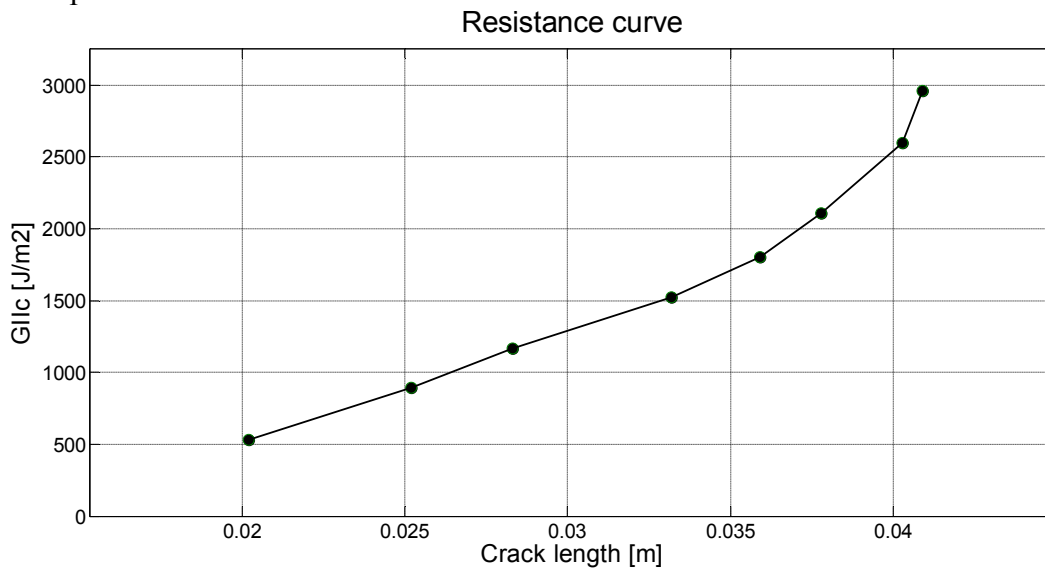

Figure 39: ENF - METU, Resistance curve

GIIc values show raising tendency with increasing crack length. This is common for ductile materials. Reason is that plastic zone at crack tip increases in size with extension. [22]

4.1 Mode I – Double cantilever beam, BUT

Fracture toughness mode I testing in BUT was performed to compare temperature effect on fracture toughness.

4.1.1 Specimen preparation

Series of specimen to investigate temperature effect for mode I were prepared.

4.1.1.1 Material

Epoxy resin MGS L 285 with activator MGS L 287 were used to impregnate unidirectional carbon sewed woven. Cloth was 200 g/m^2 specific weight, Toho Tenax fiber. Material properties are specified at Table 3.

Table 3: Material properties – BUT - Temperature effect, Toho Tenax Material properties [23]

Physical properties	Units	AGP 280-5H
Filament diameter	μm	7
Fiber density	g/cm^3	1.76
Tensile strength	MPa	3950
Tensile modulus	GPa	238
Elongation to break	%	1.7
Specific heat capacity	J/kgK	710
Thermal conductivity	W/mK	10
Coefficient of thermal expansion	$10^{-6}/K$	-0.1
Specific electrical resistance	Ω cm	$1.6\ 10^{-3}$

4.1.2 Manufacturing

Rectangular plate was prepared with $[0_6]_s$ stacking sequence using wet lamination technique. Teflon band was insert between midplane layers to ensure crack position. Plate was vacuum bagged and then cured at room temperature.
After curing, it was put into oven at temperature 60°C for 15 hours, to increase its glass transition temperature to be able to examine its effect on fracture toughness.
Plate was split into specimen using water cutting in AWAC Company.
Specimen fiber mass ratio was calculated 60.7%.

Specimens were cut according 3.1.2.
At the end Piano hinges were glued by epoxy resin MGS L 285.
One side of specimen was sprayed white.

4.1.3 Test equipment

Tests were performed on loading machine LABORTECH 6.500SP1-VM using Test and motion software. Sampling frequency was chosen 1000 Hz. Such a high frequency causes problems during data post processing later. Therefore it was reduced to 100 Hz. Photograph recording was automatized using optical extensometer system communicating with Mercury software. Photos

were taken with frequency of 5 Hz. To heat specimen LABORTECH oven was used, which is integrated in loading machine.

4.1.4 Test setup

Tests were performed on the same BUT machine and software as previous ones.
Tests were performed as described in 3.1.3.

Figure 40: DCB-BUT, Test setup – initial crack length

Figure 41: DCB-BUT, Test setup – end crack length

To achieve relevant data of specimen measured at elevated temperature it was desirable to preheat them in oven before installed into clamps to ensure proper temperature value throughout specimen during testing.

4.1.5 Experimental output

Similarly as during METU testing, load displacement curves were obtained directly from testing machine software. Then resistance curves were computed using MATLAB script.

During testing unexpected behavior was observed. Since specimen was not precracked before testing, there was still some epoxy resin connecting parts with Teflon insert. This caused steep raise of loading force before initial delamination occurs. After that force is supposed to drop down in acceptable values, however it did not.
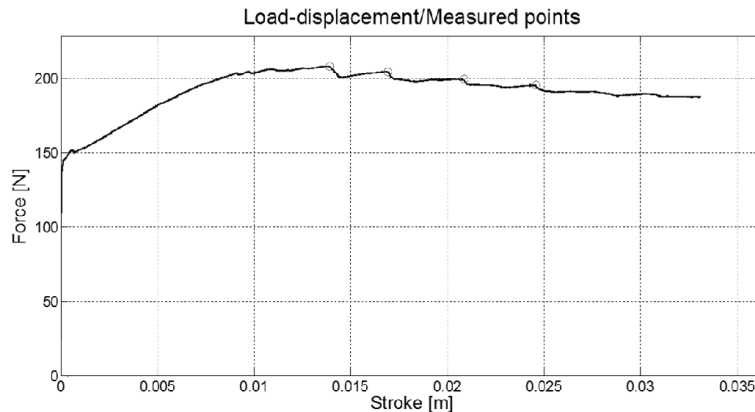

Figure 42: DCB - BUT, Load displacement curve – unrealistically high values

This caused unrealistically high values of fracture toughness.
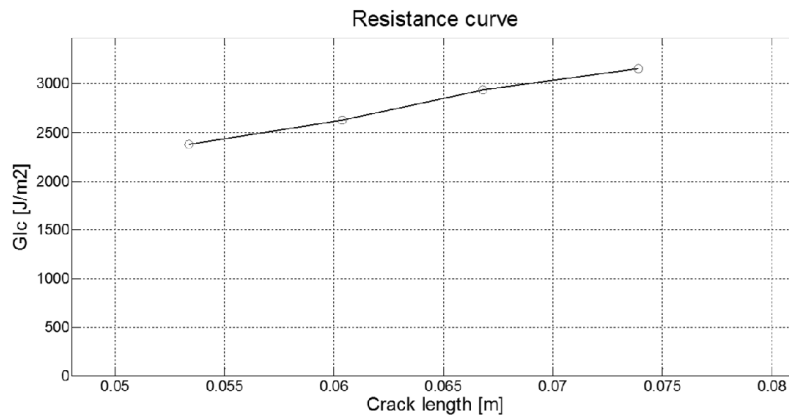

Figure 43: DCB - BUT, Resistance curve – unrealistically high values

We observed this behavior can be avoid by precracking every specimen with teflon insert using sharp wedge before it is put into testing machine.

Using this approach, the rest of specimen of this series shown reliable realistic data.

In total ten specimen were tested to examine effect of temperature. Four of them were heated at 60°C

4.2 Mode II - End notched flexure, BUT

Fracture toughness mode II testing in BUT was performed to compare fiber mass ratio effect on fracture toughness.

4.2.1 Specimen preparation – fiber mass ratio effect

4.2.1.1 Material

Epoxy resin MGS L 285, same as in previous case, with activator MGS L 284 (4 hours) were used to impregnate unidirectional carbon sewed roving. Cloth was Tenax HTA5131800tex fiber with following properties:

Table 4: Material properties – BUT – Fiber mass ratio, Tenax HTA, Material properties [24]

Physical properties	Units	AGP 280-5H
Fiber density	g/cm^3	1.78
Fiber count		8080
Tensile strength	MPa	4830
Tensile modulus	GPa	241
Elongation to break	%	2
Electrical resistivity	Ω cm	0.0015

4.2.1.2 Manufacturing

Specimen were manufactured by pressure molding -Figure 44. This process was chosen to increase fiber mass ratio in the specimen

Specimens were not primarily manufactured for fracture toughness testing. They were tested to examine bending strength of such a material. However side part of deformed specimen were not affected by test, therefore it was possible to cut these parts and use them for fracture toughness testing as well.
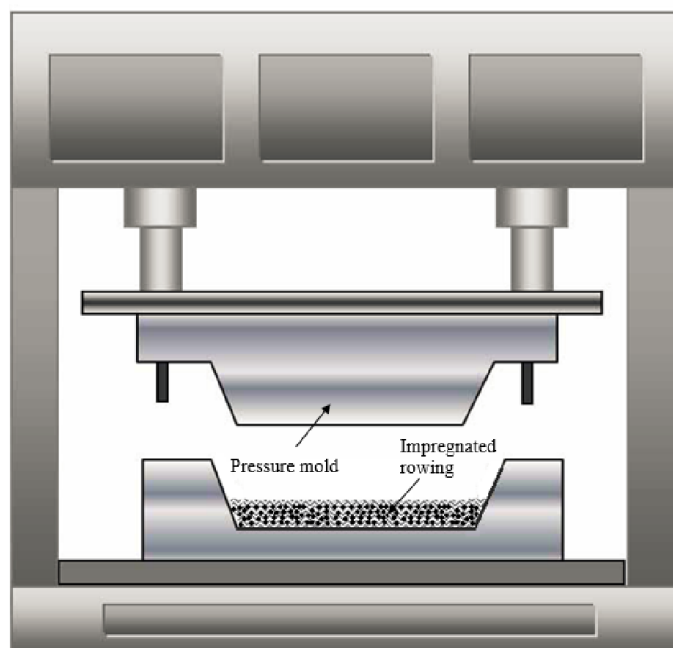
Figure 44: Specimen preparation – BUT, pressure molding

Specimen dimensions follows the rules defined in section 3.2.2.

Initial crack was created as described in ASTM DCB standards and literature [14], by using sharp wedge pushed into specimen. To obtain proper crack length the specimen sides were painted white. As shown on Figure 45 fracture testing crack did not follow the midplane.
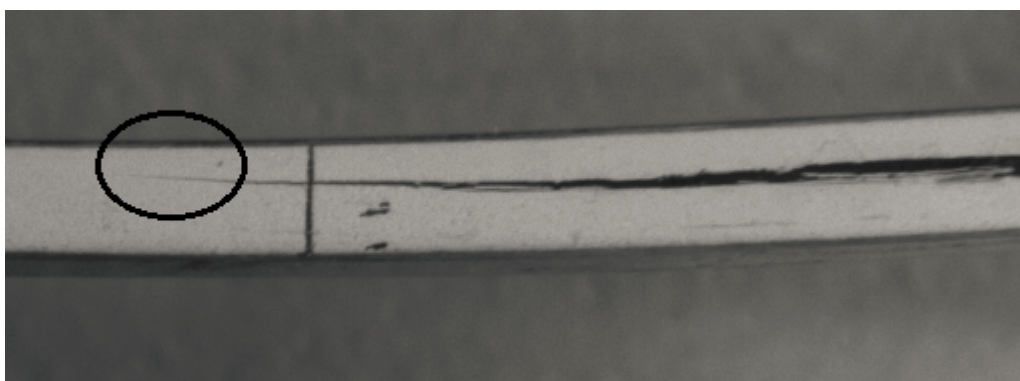

Figure 45: ENF – BUT, crack midplane deviation

This was caused by fact that they were manufactured from unidirectional roving. To prevent such a behavior from happening in future unidirectional fabric should be used instead.

4.2.2 Test setup

Tests were performed on the same equipment using same software as for mode I.
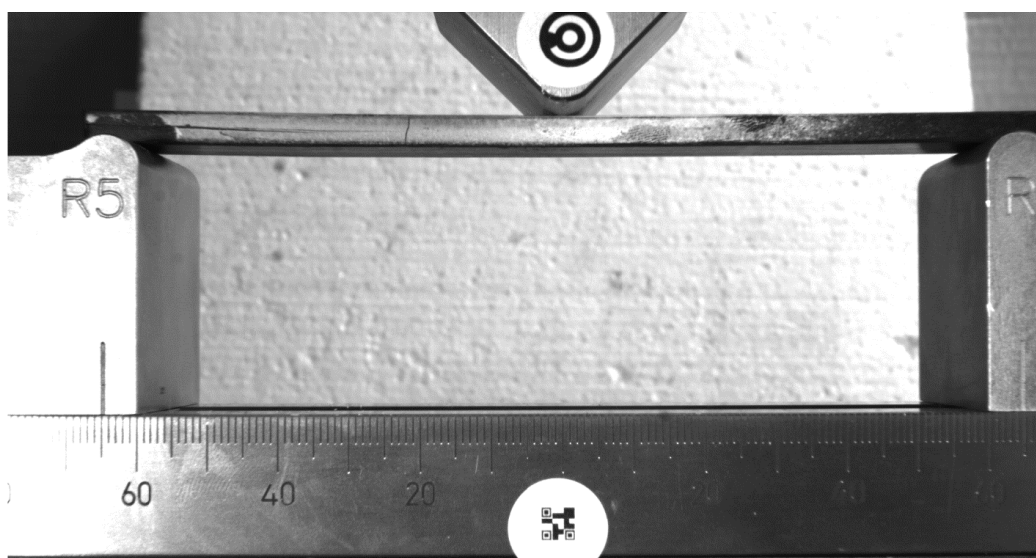Test were performed as described in section 3.2.3.

Figure 46: ENF-BUT, Test setup

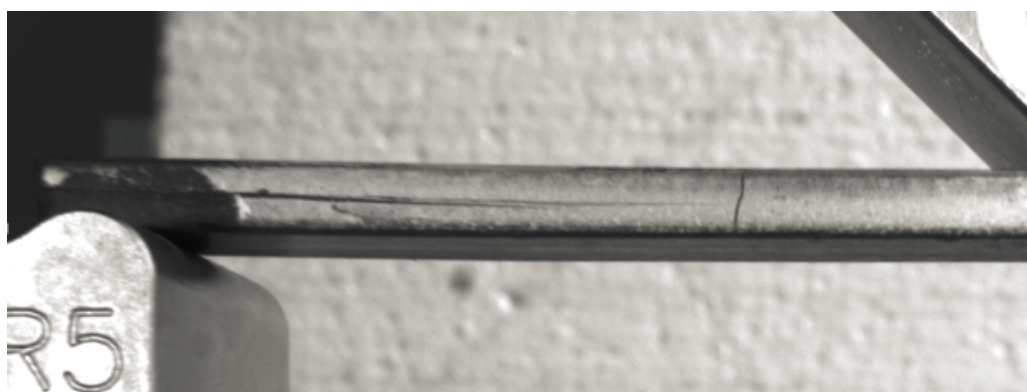Out of the first photo taken, initial crack length was measured.

Figure 47: ENF-BUT, Initial crack length

Test was stopped after 100 seconds. It was observed, during this time crack goes through desired propagation area and reaches the upper support area.
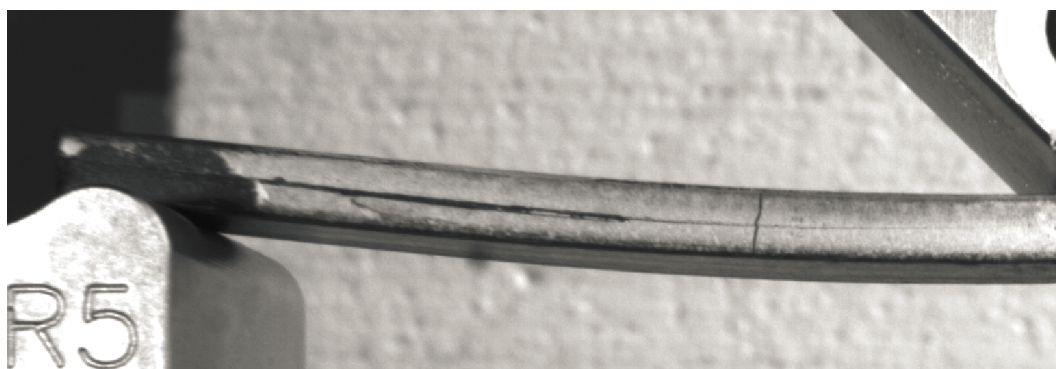

Figure 48: ENF-BUT, End crack length

Different loading speeds were applied to inspect its effect and find the ideal one for testing procedure. To preload specimen, higher speeds were used and then slowed down to be able to record stable crack growth. However this process shows difference in the load-displacement curves, which was caused probably by sliding of specimen down the support, faster when higher speed were applied.

4.2.2.1 Load displacement curve

Generally curves showed higher load drops than these obtained in METU. Therefore lesser measuring points were taken.
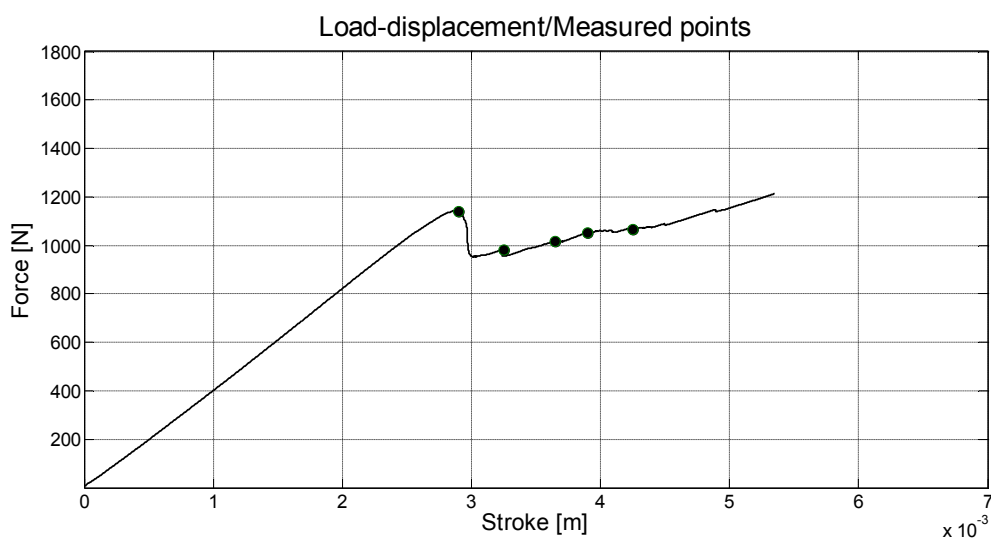

Figure 49: ENF - BUT, Load displacement curve

4.2.3 **Resistance curve**

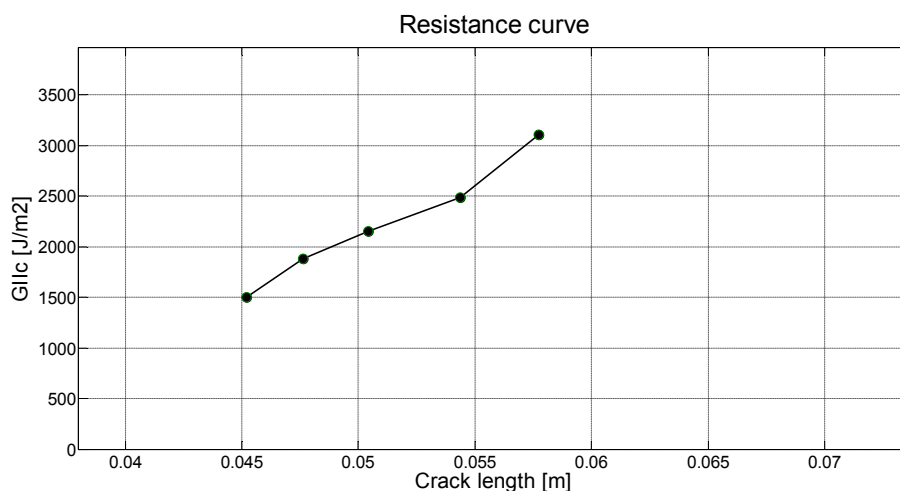Resistance curves showed reasonable values of fracture toughness.

Figure 50: ENF - BUT, Resistance curve

5. Data processing

For better understanding the whole procedure data process itself is explained step by step.

It is the most time consuming procedures during whole testing.
Raw data obtained from loading machine are saved in text document. Due to high amount of tested specimen it is more convenient to export these data into excel database. Then data is read by Matlab script and required values are calculated.

5.1 Excel database

The main reason to create database in Excel is to make values well arranged. Therefore there are standardized format of columns and rows for every single specimen.
First rows show which specimen are following data for, the date and type of the test.

Test Name	Test Date	Test Type				
1-UD,DP	15,4,2014	3 Point				

Figure 51: Excel database, Upper part

Next, it is necessary to have an opportunity to comment deviations occurred during the test.

Title	Sub title	Comment				
		Crack did not follow midplane				

Figure 52: Excel database, Middle part 1/2

At twelfth row there are numerical data of the specimen and loading machine e.g. initial crack length, width, length, thickness, loading speed and sampling frequency.

Shape:	Batch Size	SubBatch Size:				
Plate	1,0000	1,0000				
1- 1						
Size Unit:	mm	mm				
a0	w	L	t	v [mm/mi	DataFreq	
49,8100	20,4700	175,5000	3,0500	5,0000	0,0100	

Figure 53: Excel database, Middle part 2/2

The rest of database consist of loading machine data plus loading force, displacement and crack length after each propagation.

Čas	Dráha	Síla	Protažení	P	D	a
s	mm	N	mm	N	mm	mm
0	0,0072	24,53	0	208,0000	13,9200	53,3800
0,01	0,008	27,74	0	204,5000	16,9200	60,3800
0,02	0,0089	30,73	0	199,4000	20,8600	66,8000
0,03	0,0098	33,39	0	195,6000	24,5800	73,9200
0,04	0,0106	35,93	0			
0,05	0,0115	38,65	0			

Figure 54: Excel database, Lower part

It is necessary to choose proper sampling frequency to avoid too rough or too smooth data. It was observed that about ten thousand rows of data is enough.

Databases were made separately for mode I and mode II. Both are attached in appendix of this thesis.

5.2 Matlab script

Data can be processed in arbitrary computational software. Matlab was chosen due to its global popularity.

5.2.1 Mode I

Excel database is read by Matlab script to process data more efficiently.

At the beginning, all previously saved data are erased and desired specimen is chosen.

```
clc
clear all
close all

%Defines which specimen claculates data for
Sheet = 1;  %type of specimen
Mea = 1;    %specimen number
```

To computed more specimen at one time "for" cycle is used.

Then axis initial variable values are defined to get proper dimension for final graphs

```
%Axis dimension values definition
Pmax = 0;
GImax = 0;
Dmax = 0;
amax = 0;
amin = 1;
```

To be able to compute more than one specimen at time cell format is defined.

```
%Cell format definition
Load=cell(Mea,1);
P=cell(Mea,1);
D=cell(Mea,1);
a=cell(Mea,1);
Time=cell(Mea,1);
Stroke=cell(Mea,1);
photo=cell(Mea,1);
GI=cell(Mea,1);
```

Next part reads excel database values, position of every specimen.

```
%Read measured values
Load{1}=(xlsread('DCBDatabaseVUT+METU.xlsx',Sheet,'C21:C1000000'))';    %[N]
P{1}=(xlsread('DCBDatabaseVUT+METU.xlsx',Sheet,'E21:E100'))';           %[s]
D{1}=(1e-3*xlsread('DCBDatabaseVUT+METU.xlsx',Sheet,'F21:F100'))';      %[N]
a{1}=(1e-3*xlsread('DCBDatabaseVUT+METU.xlsx',Sheet,'G21:G100'))';      %[mm]
a0(1)=1e-3*xlsread('DCBDatabaseVUT+METU.xlsx',Sheet,'A12');
b(1)=1e-3*xlsread('DCBDatabaseVUT+METU.xlsx',Sheet,'B12');
L(1)=1e-3*xlsread('DCBDatabaseVUT+METU.xlsx',Sheet,'C12');
h(1)=1e-3/2*xlsread('DCBDatabaseVUT+METU.xlsx',Sheet,'D12');
v(1)=xlsread('DCBDatabaseVUT+METU.xlsx',Sheet,'E12');
DataFreq(1)=xlsread('DCBDatabaseVUT+METU.xlsx',Sheet,'F12');

Load{2}=(xlsread('DCBDatabaseVUT+METU.xlsx',Sheet,'K21:K1000000'))';    %[N]
P{2}=(xlsread('DCBDatabaseVUT+METU.xlsx',Sheet,'M21:M100'))';           %[s]
D{2}=(1e-3*xlsread('DCBDatabaseVUT+METU.xlsx',Sheet,'N21:N100'))';      %[N]
a{2}=(1e-3*xlsread('DCBDatabaseVUT+METU.xlsx',Sheet,'O21:O100'))';      %[mm]
.
.
.
```

Out of the time values and loading speed stroke is computed.

```
%Stroke computation
for i=1:Mea
Time{i}=DataFreq(i):DataFreq(i):length(Load{i})*DataFreq(i);
Stroke{i}=Time{i}*10^-3*v(i)/60;
End
```

For every crack propagation point relevant photo is accessed.

```
%photo pickup
for i=1:Mea;
    for j=1:length(D{i});
        temp=D{i};
        phot(j)=round(temp(j)*1000/v(i)*60*DataFreq(i));
    end
     photo{i}=phot;
     phot=0;
end
```

Fracture toughness itself is calculated next.

```
%Fracture toughness
for i=1:Mea
    Ptemp=P{i};
    Dtemp=D{i};
    atemp=a{i};
    clear F;
    %Compliance curve creation
    for j=1:length(Ptemp)
        C(j)=(Dtemp(j)/Ptemp(j));                        %Compliance
        C13(j)=C(j)^(1/3);
        F(j)=1-3/10*(Dtemp(j)/atemp(j))^2-3/2*(Dtemp(j)*t/atemp(j)^2);
%Large displacement effect coefficient
    end
        %Trendlines
        X=-10:0.01:10;              %Trendline range

        %MTB
        p=polyfit(atemp,C13,1);     %Makes linear trendline of
compliance/crack length graph
        delt=-p(2)/p(1);            %Delta correction factor
        CMTB=polyval(p,X);          %Trendline values

        %CC
        p=polyfit(log(atemp),log(C),1);
        n=p(1);                     %n exponent for CC method
        CCC=polyval(p,X);

        %MCC
        p=polyfit(C13,atemp/h(i),1);
        A1=p(1);                    %Slope of trendline
        MCC=polyval(p,X);

    for j=1:length(Ptemp)
        %Fracture toughness
        GIMBT(j)=3*Ptemp(j)*Dtemp(j)/(2*b(i)*(atemp(j)-delt))*F(j);
%Interlaminar fracture toughness MODE I (MTB method)
        GICC(j)=n*Ptemp(j)*Dtemp(j)/(2*b(i)*atemp(j))*F(j);
%Interlaminar fracture toughness MODE I (CC method)
        GIMCC(j)=3*Ptemp(j)^2*C(j)^(2/3)/(2*A1*b(i)*h(i))*F(j);
%Interlaminar fracture toughness MODE I (MCC method)

        if  GIMBT(j) > GImax;
            GImax = GIMBT(j);
        end

        if  Ptemp(j) > Pmax;
            Pmax = Ptemp(j);
        end

    Dmaxtemp = length(Load{i})*DataFreq(i)*v(i)/60*10^-3;

        if  Dmaxtemp > Dmax;
            Dmax = Dmaxtemp(i);
        end

        if  atemp(j) > amax;
```

```
        amax = atemp(j);
    end

    if  atemp(j) < amin;
        amin = atemp(j);
    end
    end
    GIm(i)=mean(GIMBT);
    GIsd(i)=std(GIMBT);
    GI{i}=GIMBT;
    GIMBT=0;
    C13=0;
    C=0;
    F=0;
end
```

During computation maximum and minimum data values are stored to ensure proper dimensions of final graphs

At the end load-displacement and resistance curves are plotted.

```
%Plot
for i=1:Mea
marker=['--';'-.';'-o';'-x';'-+';'-*';'-d';'-:';'-s'];
color = ['b';'g';'r';'c';'m';'y';'k';'b';'g'];

figure(1)
plot(Stroke{i},Load{i},marker(i),'color',color(i),'Linewidth',2);
title('Load-displacement/Measured points'); xlabel('Stroke
[m]');ylabel('Force [N]');grid ON; axis([0 1.1*Dmax 0 1.1*Pmax]), hold on
scatter(D{i},P{i},100)

figure(2)
plot(a{i},GI{i},marker(i),'color',color(i),'Linewidth',2); title('Resistance
curve'); xlabel('Crack length [m]');ylabel('GIc [J/m2]');grid ON;
axis([0.9*amin 1.1*amax 0 1.1*GImax]), hold on
scatter(a{i},GI{i},100)
end
```

Finally fracture toughness mean values are displayed.

```
%Disp
disp('Mean interlaminar fracture toughness MODE II:')
GIm     %Mean interlaminar fracture toughness MODE I (MTB method)
disp('Standart deviation GI:')
GIsd    %Standart deviation
```

5.2.2 **Mode II**

Most of the script is similar for each modes. Only part contains calculation itself is different.

```
%Calculation
%Fracture toughness
for i=1:Mea
    Ptemp=P{i};
    Dtemp=D{i};
    atemp=a{i};
    for j=1:length(Ptemp);

GIItemp(j)=9*atemp(j)^2*Ptemp(j)*Dtemp(j)/(2*b(i)*(2*L(i)^3+3*atemp(j)^3));
%#ok<SAGROW> %Interlaminar fracture toughness MODE I (MTB method)

        if  GIItemp(j) > GIImax;
            GIImax = GIItemp(j);
        end

        if  Ptemp(j) > Pmax;
            Pmax = Ptemp(j);
        end

    Dmaxtemp=length(Load{i})*DataFreq*v(i)/60*10^-3;
        if  Dmaxtemp > Dmax;
            Dmax = Dmaxtemp(j);
        end

        if  atemp(j) > amax;
            amax = atemp(j);
        end

        if  atemp(j) < amin;
            amin = atemp(j);
        end

    end
    GIIm(i)=mean(GIItemp);
    GIIsd(i)=std(GIItemp);
    GII{i}=GIItemp;
    GIItemp=0;
end
```

Both script is add in appendix of this thesis.

6. Discussion

In this chapter results are presented and put into context with the ones found in literature. Possible discrepancies are commented and suggestion how to avoid them in the future are made.

Based on obtained experimental results the actual effect of CNTs, fiber mass ratio and manufacturing technology are described. General conclusions for each of them are deduced and compared to the expectations.

6.1 Effect of CNTs

As mentioned in section 2.3.3 CNTs additive are expected to have significant effect in fracture toughness of CFRP.

Therefore its effect is tested.

6.1.1 Mode I – DCB

Specimen with and without CNTs were tested for fabric and rowing material. In total four specimen were tested

6.1.1.1 Load-displacements curves
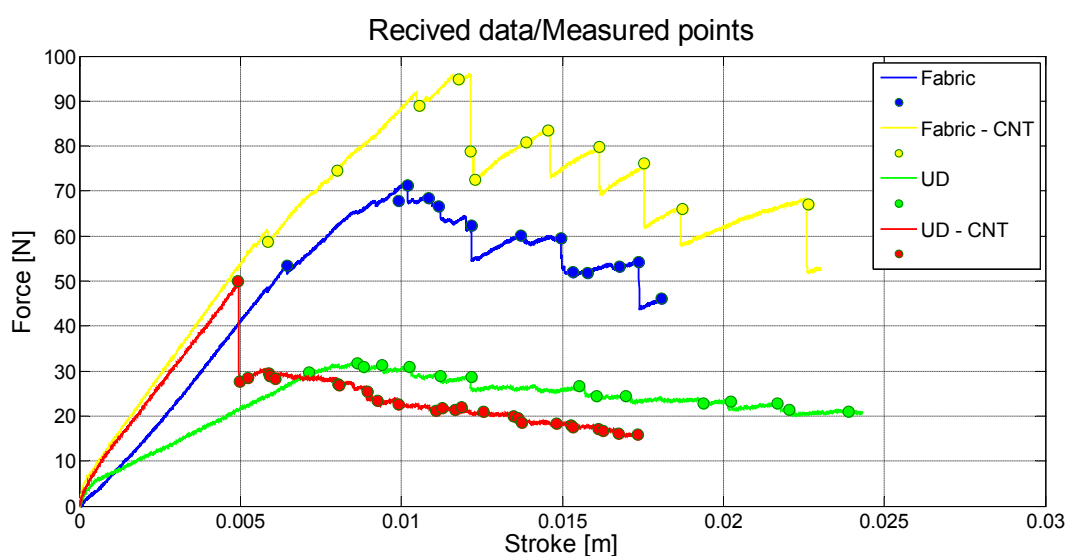
Figure 55: DCB, Effect of CNTs, Load - displacement curves

CNT fabric was able to transmit highest value of force before failure.

6.1.1.2 Resistance curves
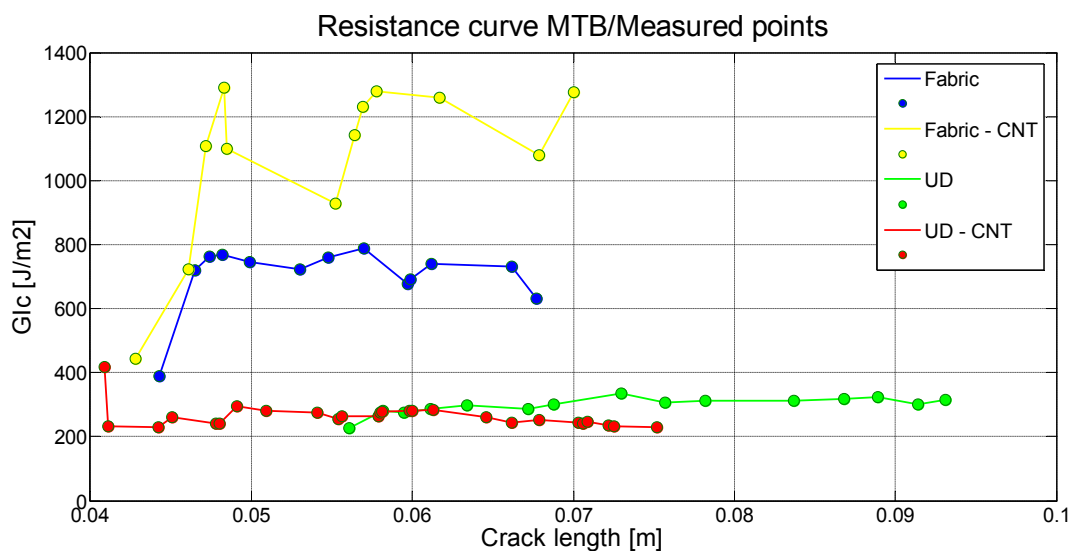
Figure 56: DCB, Effect of CNTs, Resistance curves

Since crack lengths were similar for most of specimens, fracture values represents load displacement curves.

6.1.1.3 Results

Table 5: Effect of CNTs, DCB Results

Specimen	Meas. points	Mean $G_{IC}MBT$	Mean $G_{IC}CC$	Mean $G_{IC}MCC$	Standard deviation
Fabric CNT	12	1 071.5	1 060.3	1 108.9	227.4
Fabric	18	735.6	733.3	745.7	97.5
UD CNT	15	298.6	300.1	301.3	25.7
UD	26	263.2	269.0	271.2	37.0

Results values are similar to ones shown in literature. [25]
Since results are almost the same for every computation method for next time the MBT approach is used only.

6.1.2 **Mode II – ENF**

Fabric specimen only were tested for mode II. Again four specimen were tested in total. Two of them contained CNTs

6.1.2.1 Load-displacements curves
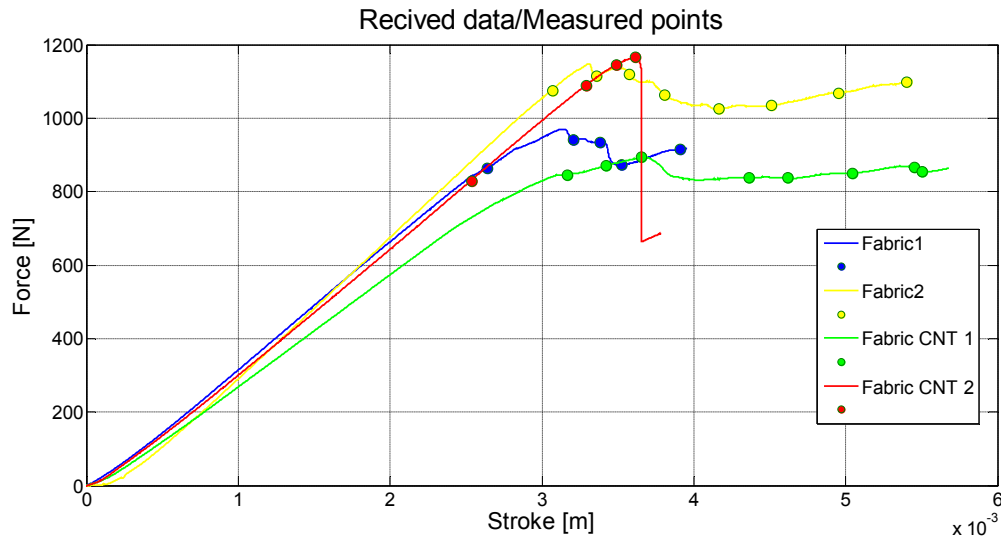
Figure 57: ENF, Effect of CNTs, Load - displacement curves

Fabric CNT 2 specimen failed in undesired way, which leaded to irrelevant data.
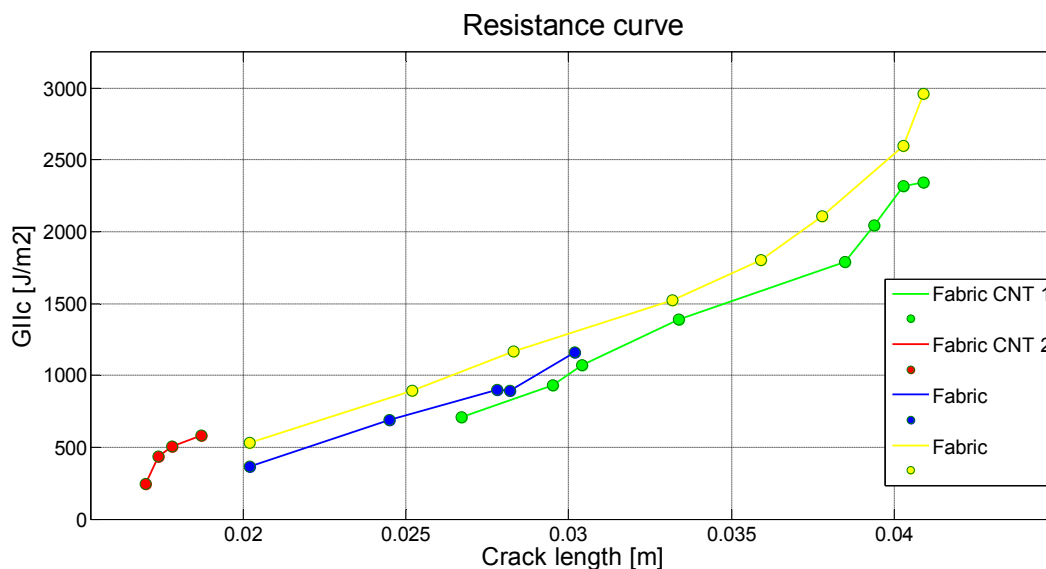
6.1.2.2 Resistance curves

Figure 58: ENF, Effect of CNTs, Resistance curves

Again resistance curve showed that Fabric CNT 2 specimen fracture toughness is inaccurate.

6.1.2.3   Results

Table 6: Effect of CNTs, ENF Results

Specimen	Meas. points	Mean G_{IIC}	Standard deviation
Fabric 1	5	800	296
Fabric 2	8	1697	836
Fabric CNT 1	8	1574	639
Fabric CNT 2	4	440	145

High standard deviation value and significant differences between single specimens indicate that obtained data are not reliable enough.

However results values are similar order to ones shown in literature. [16]

Experiments show unexpected effect of CNTs. Even they were spread evenly on carbon/epoxy composite, during curing process they reposition and concentrate in **clusters** with high density of CNTs. This was proved also by specimen observation after testing.

CNTs concentrators caused **heterogeneous** ply with **non-isotropic** mechanical properties, which causes high load drops of CNTs included specimens during loading. This effect makes such a laminate behavior **unpredictable** – not convenient for engineering design.

Therefore U/D laminates with CNTs show lower G_{IC} and G_{IIC} values than ones without. However cross-ply laminates G_{IC} and G_{IIC} values were increased by adding CNTs. Unfortunately even there were observed **higher load drops** during testing.

It is assumed that cluster effect was caused by inconvenient methanol treatment procedure before the testing. [26]

6.2 **Effect of ply structure**

As mentioned in literature, there is fracture toughness value difference when crack occurs between two unidirectional roving and or fabric plies.

6.2.1 **Mode I - DCB**

To confirm these hypothesis several mode I DCB specimens made from UD fabric in BUT and UD roving in METU were compared.
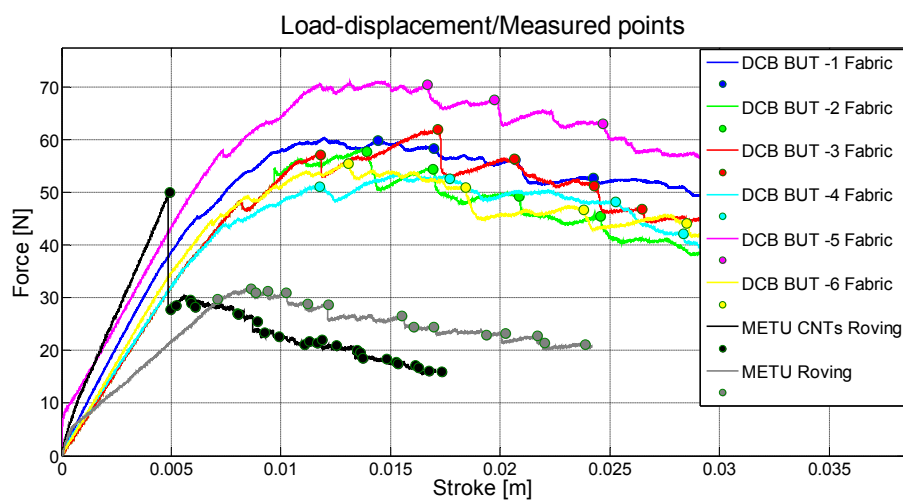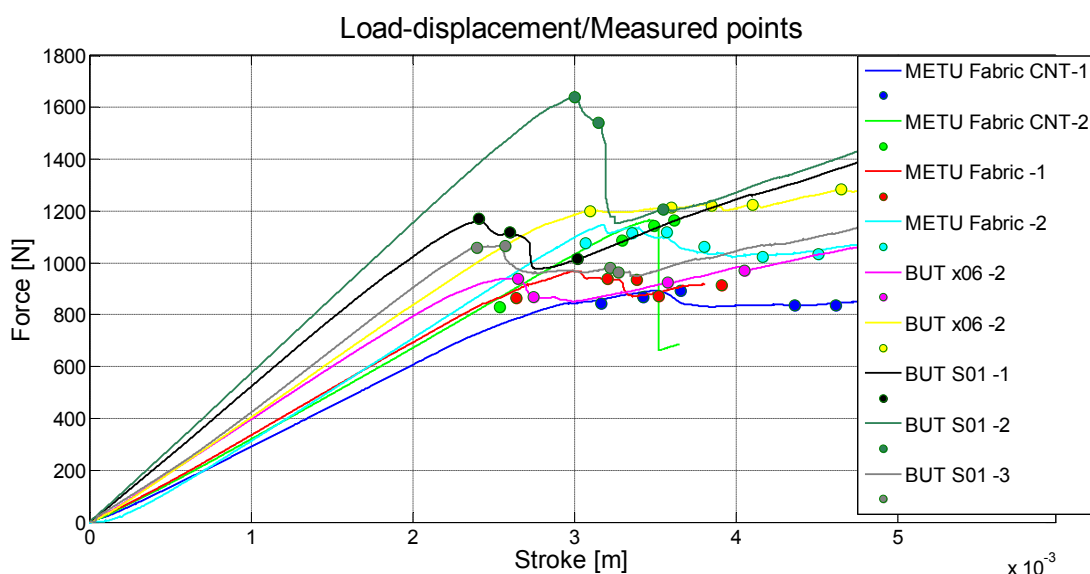
6.2.1.1 Load-displacements curve.

Figure 59: Effect of ply structure, DCB – BUT + METU, Load – displacement curves

Generally, Fabric specimen were able to transmit much higher load than roving ones

6.2.1.2 Resistance curves
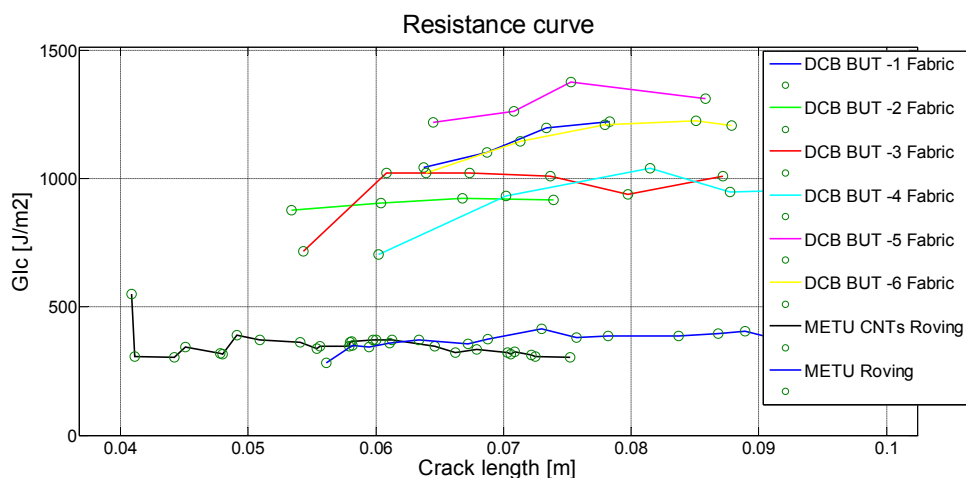
Figure 60: Effect of ply structure, DCB – BUT + METU, Resistance curves

Graphs shows significant difference between UD roving and UD fabric. Results

58

Table 7: Effect of ply structure, DCB Results

Specimen	Meas. points	Mean G$_{IIC}$	Standard deviation	Fabric/Roving
DCB-BUT1	4	1 141	83.67	Fabric
DCB-BUT2	4	906	19.63	Fabric
DCB-BUT3	6	953	119.4	Fabric
DCB-BUT4	5	951	125.5	Fabric
DCB-BUT5	4	1 292	67.19	Fabric
DCB-BUT6	5	1 161	84.2	Fabric
METU UD CNT	15	298.6	25.7	Roving
METU UD	26	263.2	37.0	Roving

Specimen made of fabric show much higher fracture toughness value than roving ones. This observation corresponds with these mentioned in literature.

6.2.2 Mode II - ENF

Similar procedure was performed for mode II.

To confirm these hypothesis several mode II ENF specimens made from UD roving in BUT and UD fabric in METU were compared.

6.2.2.1 Load-displacements curve

Figure 61: Effect of ply structure, ENF – BUT + METU, Load – displacement curves

Load difference for mode II is not as evident as in mode I case.
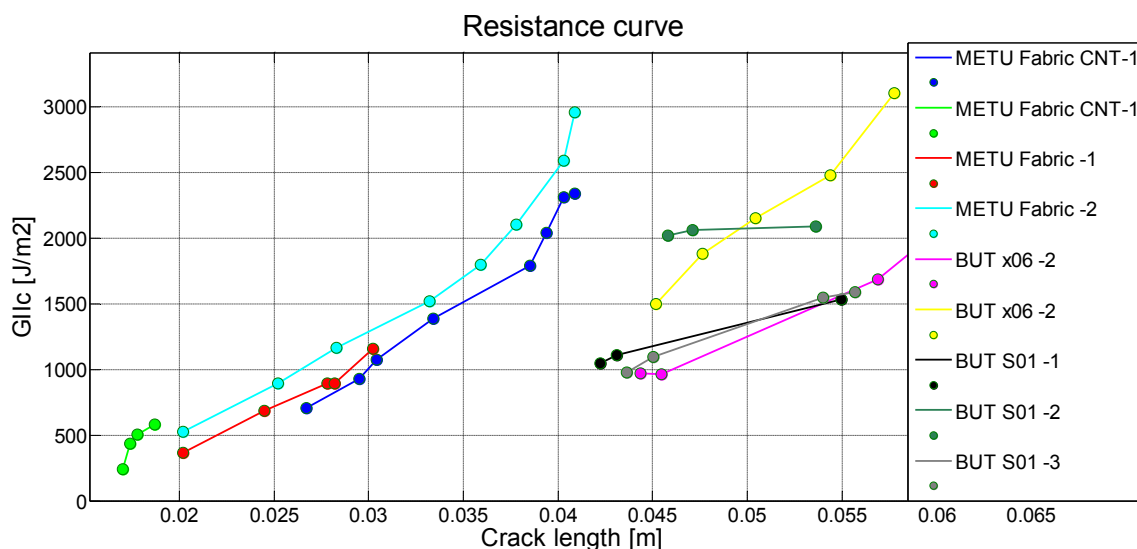
6.2.2.2   Resistance curves

Figure 62: Effect of ply structure, ENF – BUT + METU, Resistance curves

Again graphs shows higher values for fabric specimen.

6.2.2.3   Results

Table 8: Effect of ply structure, ENF Results

Specimen	Meas. points	Mean G_{IIC}	Standard deviation	Fabric/Roving
METU Fabric -1	5	800	639	Fabric
METU Fabric -2	8	1697	145	Fabric
METU Fabric CNT -1	8	1574	296	Fabric
METU Fabric CNT -2	4	440	836	Fabric
x06_73,7 – 2	4	1 427	554.6	Roving
x06_73,7 – 3	5	2 226	609.7	Roving
S01_69,6 – 1	3	1 223	265.8	Roving
S01_69,6 – 2	3	2 058	34.53	Roving
S01_69,6 – 3	4	1 304	310.0	Roving

Ply structure specifically the fact if part is made of roving or fabric has high impact on its fracture toughness. Difference is more distinct for mode I.

6.3 **Effect of fiber mass ratio**

Fiber mass ratio effect was observed at mode II ENF specimens.

In literature, it is mention that fracture toughness is decreasing while fiber mass ratio is higher, therefore it was necessary to confirm such an effect. [27]

Three series of specimen with different fiber mass ratio were prepared with three pieces in each of them.
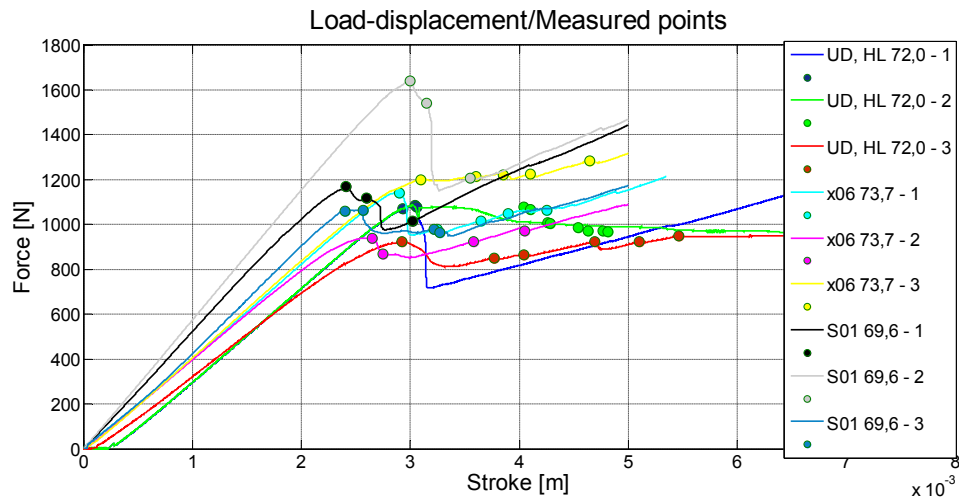
6.3.1.1   Load-displacements curves

Figure 63: Effect of fiber mass ratio, ENF – BUT, Load – displacement curves

Load-displacement curves showed no significant difference between these series.

6.3.1.2   Resistance curves
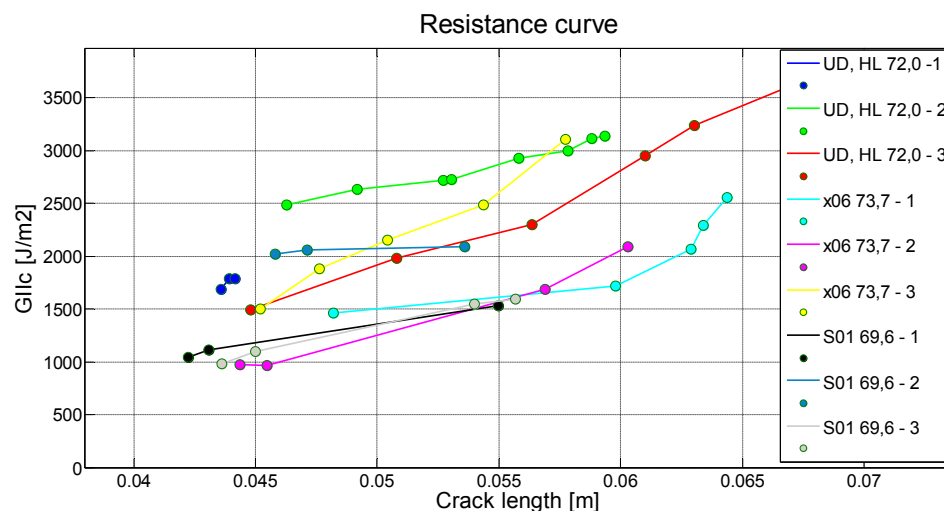
Figure 64: Effect of fiber mass ratio, DCB – BUT, Resistance curves

Resistance curves showed no difference either.

Table 9: Effect of fiber mass ratio, ENF – BUT

Specimen	Meas. points	Mean G_{IIC}	Standard deviation	Fiber mass ratio
UD,HL_72,0 – 1	3	1 752	59.64	72%
UD,HL_72,0 – 2	8	2 841	236.9	72%
UD,HL_72,0 – 3	6	2 593	806.9	72%
x06_73,7 – 1	5	2 016	438.4	73,7%
x06_73,7 – 2	4	1 427	554.6	73,7%
x06_73,7 – 3	5	2 226	609.7	73,7%
S01_69,6 – 1	3	1 223	265.8	69,6%
S01_69,6 – 2	3	2 058	34.53	69,6%
S01_69,6 – 3	4	1 304	310.0	69,6%

Unlike in literature our measurement did not show any connections between fiber mass ratio and fracture toughness.

However, since standard deviation reaches relatively high values and on the other hand the fiber mass ratio differences is few percent only the effect itself can be hidden in deviation.

6.4 **Effect of temperature**

6.4.1 **Mode I**

6.4.1.1 Load-displacements curves
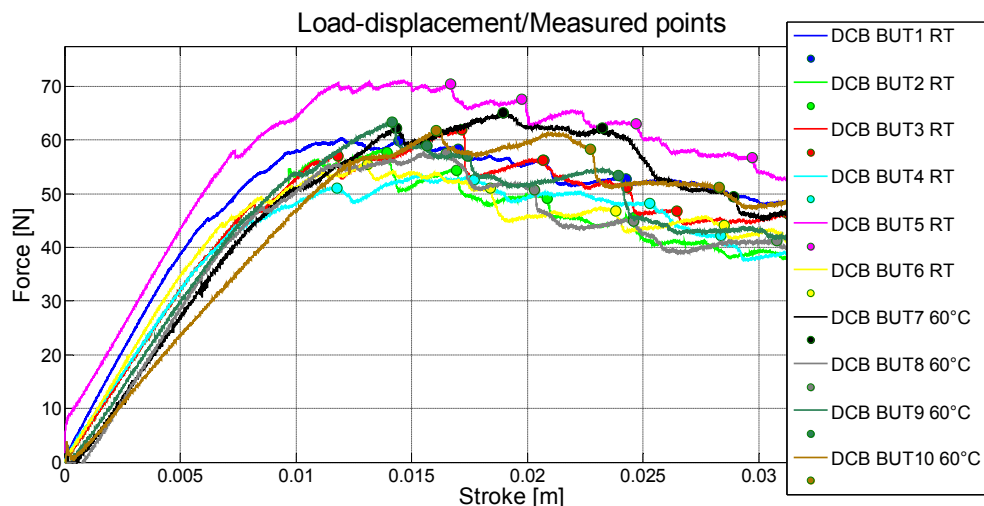
Figure 65: Effect of temperature, DCB – BUT, Load - displacement curves

Load displacement curves does not show any temperature effect. For both specimens, at room temperature and heated ones, crack starts to propagate at same loading force.
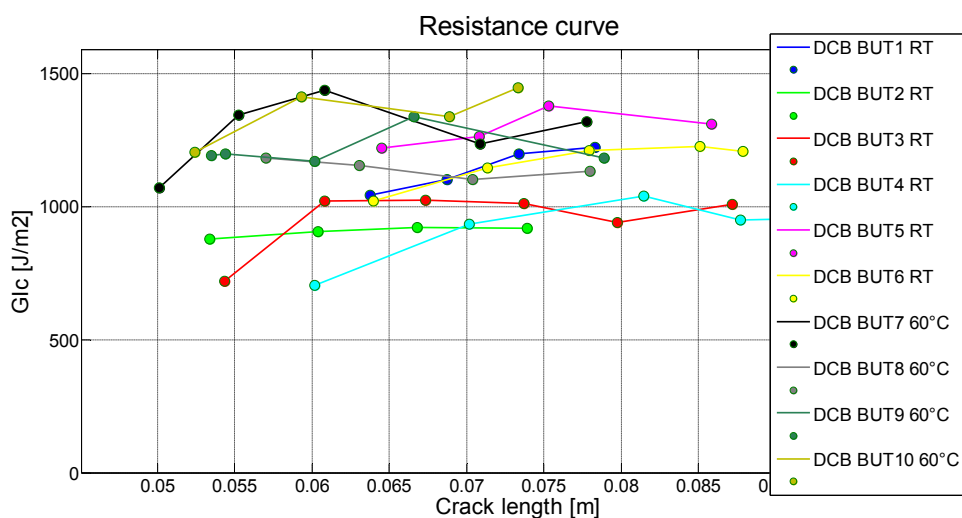
6.4.1.2 Resistance curves

Figure 66: Effect of temperature, DCB – BUT, Resistance curves

However, resistance curves showed unexpected results. Heated specimens showed slower crack growth at same load. Therefore they reaches higher fracture toughness values.

Table 10: Effect of temperature, DCB Results

Specimen	Meas. points	Mean G_{IIC}	Standard deviation	Temp.
DCB-BUT1	4	1 141	83.67	Room Temp.
DCB-BUT2	4	906	19.63	Room Temp.
DCB-BUT3	6	953	119.4	Room Temp.
DCB-BUT4	5	951	125.5	Room Temp.
DCB-BUT5	4	1 292	67.19	Room Temp.
DCB-BUT6	5	1 161	84.2	Room Temp.
DCB-BUT7	5	1280	138.9	60°C
DCB-BUT8	4	1142	33.8	60°C
DCB-BUT9	5	1215	69.4	60°C
DCB-BUT10	4	1349	107.8	60°C

As shown at Table 10 heated specimens have approximately 10-20% higher fracture toughness than room temperature ones.

It is assumed that elevated temperature affects plastic crack tip region positively in terms of its ductility. Therefore, to make crack pass more ductile region more energy is spent.

However this fact does not match with literature where it is mentioned in that interlaminar fracture toughness decreased with an increase in temperature. [28]

6.5 **Effect of loading mode**

It is important to note that loading mode itself has main effect on under which conditions crack propagation occurs.

This effect was proven during tests throughout all specimen.

Table 11: Effect of loading mode

Specimen	Meas. points	Mean G_{IIC}	Standard deviation	Mode
DCB-BUT1	4	1 141	83.67	I
DCB-BUT7 60°C	5	1280	138.9	I
METU UD CNT	15	298.6	25.7	I
METU UD	26	263.2	37.0	I
Fabric CNT	12	1 071.5	227	I
UD,HL_72,0 – 1	3	1 752	59.64	II
x06_73,7 – 1	5	2 016	438.4	II
S01_69,6 – 1	3	1 223	265.8	II
METU Fabric -1	5	1574	639	II
METU Fabric CNT -1	8	800	107.8	II

6.6 **Summary**

Finally, all measured specimen result data are presented together in one table. The most important facts are noted.

Table 12: Summary

Spec.	Mean G_{IC}	Standard deviation	Mode	Fiber mass ratio	Manufacturing technology	Fabric / Roving	Temp.	CNT Y/N
Fabric CNT	**1 071.5**	227.4	I	55.3%	Prepreg Autoclave	0/90 Fabric	RT	Y
Fabric	**735.6**	97.5	I	55.3%	Prepreg Autoclave	0/90 Fabric	RT	N
UD CNT	**298.6**	25.7	I	57.4%	Prepreg Autoclave	U/D Roving	RT	Y
UD	**263.2**	37.0	I	57.4%	Prepreg Autoclave	U/D Roving	RT	N
DCB-BUT1	**1 141**	83.67	I	60.7%.	Wet lay-up Vacuum bag	U/D Fabric	RT	N
DCB-BUT2	**906**	19.63	I	60.7%.	Wet lay-up Vacuum bag	U/D Fabric	RT	N
DCB-BUT3	**953**	119.4	I	60.7%.	Wet lay-up Vacuum bag	U/D Fabric	RT	N
DCB-BUT4	**951**	125.5	I	60.7%.	Wet lay-up Vacuum bag	U/D Fabric	RT	N
DCB-BUT5	**1 292**	67.19	I	60.7%.	Wet lay-up Vacuum bag	U/D Fabric	RT	N
DCB-BUT6	**1 161**	84.2	I	60.7%.	Wet lay-up Vacuum bag	U/D Fabric	RT	N
DCB-BUT7	**1280**	138.9	I	60.7%.	Wet lay-up Vacuum bag	U/D Fabric	60°C	N
DCB-BUT8	**1142**	33.8	I	60.7%.	Wet lay-up Vacuum bag	U/D Fabric	60°C	N
DCB-BUT9	**1215**	69.4	I	60.7%.	Wet lay-up Vacuum bag	U/D Fabric	60°C	N
DCB-BUT10	**1349**	107.8	I	60.7%.	Wet lay-up Vacuum bag	U/D Fabric	60°C	N
Fabric 1	**800**	296	II	55.3%	Prepreg Autoclave	0/90 Fabric	RT	N
Fabric 2	**1697**	836	II	55.3%	Prepreg Autoclave	0/90 Fabric	RT	N

Fabric CNT 1	**1574**	639	II	55.3%	Prepreg Autoclave	0/90 Fabric	RT	Y
Fabric CNT 2	**440**	145	II	55.3%	Prepreg Autoclave	0/90 Fabric	RT	Y
UD,HL – 1	**1 752**	59.64	II	72%	Pressure molding	U/D Roving	RT	N
UD,HL 2	**2 841**	236.9	II	72%	Pressure molding	U/D Roving	RT	N
UD,HL 3	**2 593**	806.9	II	72%	Pressure molding	U/D Roving	RT	N
x06 – 1	**2 016**	438.4	II	73,7%	Pressure molding	U/D Roving	RT	N
x06 – 2	**1 427**	554.6	II	73,7%	Pressure molding	U/D Roving	RT	N
x06 – 3	**2 226**	609.7	II	73,7%	Pressure molding	U/D Roving	RT	N
S01 – 1	**1 223**	265.8	II	69,6%	Pressure molding	U/D Roving	RT	N
S01 – 2	**2 058**	34.53	II	69,6%	Pressure molding	U/D Roving	RT	N
S01 – 3	**1 304**	310.0	II	69,6%	Pressure molding	U/D Roving	RT	N

7. Conclusion

Global interlaminar fracture toughness analysis of carbon fiber reinforced plastics for loading mode I and II was conducted.

Tests were explained and performed for diverse conditions. Five different conditions were inspected.

First effect of CNTs was tested for both modes. No direct effect on fracture toughness was proven. CNT specimen showed higher load drops and unpredictable behavior in general. However it is necessary to note that CNT specimen showed poor material condition. Therefore it is assumed it can be avoid by proper manufacturing technology during future testing.

Next ply structure effect was studied for both modes. Fracture toughness values differs significantly for roving and fabric material structure. Fabric ones showed 30-90% higher values. Also in fabric specimen crack followed its midplane while in roving ones it traveled throughout its thickness. Since fundamental airplane composite parts such as wing beams are mostly made of roving, this fact has to be taken into account during damage tolerance design of such part.

It was desirable to verify if there is any connection between fracture toughness and fiber mass ratio. Tested specimens have shown no such effect. Range of 4.1% fiber mass ratio difference was examined. It is believed even if wider range would be tested it would show only insignificant change in value of fracture toughness.

Then temperature effect on fracture toughness for mode I was inspected. It shows unexpected results. When heated at 60°C specimen reached 10-20% higher fracture toughness. It is believed that elevated temperature has positive effect on ductility of crack tip plastic region. Therefore more energy has to be spent to make crack pass throughout this region. It would be useful to examine this effect more carefully by future testing.

Last but not least, it is necessary to note that loading mode has still main effect on fracture toughness. Generally part loaded under mode II – sliding, consumes approximately two times more energy while crack propagates compare to same part loaded under mode I opening. It was proven throughout testing of all specimen. This has to be considered during all composite damage tolerance parts design.

Based on these facts it is recommended to continue this research as follows:

- Optimize manufacturing technology of CNT composite implementing and examine its effect again.
- Test specimen for several different elevated temperature and confront results with other mechanical properties.
- Verify if there is any connection between interlaminar shear strength and fracture toughness.

8. References

8.1 Literature

[1]   Board, National Transportation Safety. *Aircraft accident report: Aloha Airlines, Flight 243, Boeing 737-200, N73711.* s.l. : NTSB, April 28, 1988.

[2]   *Damage tolerance of aircraft panels.* de Castro, Tavares, Richter-Trummer, de Matos, Moreira, da Silva. s.l. : Mecánica Experimental, 2010.

[3]   Vlček, Dalibor. *Master`s thesis: DAMAGE TOLERANCE EVALUATION OF L410 NG AIRCRAFT LOWER WING INTEGRALLY STIFFENED PANEL.* Brno : s.n., 2013.

[4]   Wikipedia. Fracture mechanics. *Wikipedia.* [Online] 3 1, 2014. [Cited: 2 2, 2014.] http://en.wikipedia.org/wiki/Fracture_mechanics.

[5]   Sanford, R. J. *Principles of fracture mechanics.* 2003 .

[6]   Wikipedia. Stress intensity factor. *Wikipedia.* [Online] 1 30, 2014. [Cited: 2 2, 2014.] http://en.wikipedia.org/wiki/Stress_intensity_factor.

[7]   http://en.wikipedia.org/wiki/Fracture_toughness. Fracture toughness. *Wikipedia.* [Online] 2 2, 2014. [Cited: 11 23, 2013.] http://en.wikipedia.org/wiki/Fracture_toughness.

[8]   *Roles of interfaces between carbon fibers and epoxy matrix on interlaminar fracture toughness of composites.* SOO-JIN PARK, MIN-KANG SEO and JAE-ROCK LEE. Daejeon, Korea : s.n., 2005.

[9]   CompMechLab Experience. [Online] CompMechLab. [Cited: 2 2014, 3.]
        http://www.eng.fea.ru/industry/composites-16/.

[10]   *Investigation of fiber bridging in double cantileaver beam specimens.* W. S.
        Johnson, P.D. Mangalgiri. Hampton, Virginia : Nasa Technical Memorandum,
        1986.

[11]   *Carbon Nanotubes: Potential Benefits and Risks of Nanotechnology in Nuclear
        Medicine.* Reilly, Raymond M. Toronto, Ontario, Canada : University of Toronto,
        2007 .

[12]   Boughton, Edward. Wolfson Centre for Materials Processing. *Brunel University
        London.* [Online] [Cited: 2 13, 2014.]
        http://www.brunel.ac.uk/wolfson/people/phd-students/edward-boughton.

[13]   doc. Ing. Josef Klement, CSc. *Nanocomposites - OLR Presentation.* 2012.

[14]   *Standart Test Method for Mode I Interlaminar Fracture Toughness of
        Unidirectional Fiber - Reinforced Polymer Matrix Composites.* ASTM. 2007.

[15]   *CHARACTERIZATION OF INTERLAMINAR FRACTURE TOUGHNESS OF A
        CARBON/EPOXY COMPOSITE MATERIAL.* Zhu, Ye. 2009.

[16]   Masahiro Araia, Yukihiro Noro, Koh-ichi Sugimoto, Morinobu Endo. *Mode I and
        mode II interlaminar fracture toughness of CFRP laminates toughened by carbon
        nanofiber interlayer.* 2007.

[17]   *ON THE MEASUREMENT OF MODE II INTERLAMINAR FRACTURE
        ENERGIES.* Russell, Alan J. 1982.

[18]   *HexPly Prepreg Technology.* HEXEL. 2013.

[19]   *Dispersion of Carbon Nanotubes in Liquids.* Jenny Hilding, Eric A. Grulke, Z. George Zhang, Fran Lockwood. Kentucky, USA : s.n., 2003.

[20]   *HexPly 8552 epoxy matrix (180°C/356°F curing matrix) - Product Data.* HexCel.

[21]   SHIMADZU. *Autograph AG-X plus Series.*

[22]   Crack growth resistance curve. *Wikipedia.* [Online] [Cited: 5 17, 2014.] http://en.wikipedia.org/wiki/Crack_growth_resistance_curve.

[23]   GmbH, Toho Tenax Europe. Havel-composites/proddocs. *Havel-composites.* [Online] [Cited: 4 15, 2014.] http://www.havel-composites.com/proddocs/HTA%20en%202011-04.pdf.

[24]   matweb.com. Material property data. *MatWeb.* [Online] [Cited: 5 21, 2014.] http://www.matweb.com/search/datasheet.aspx?matguid=7fd312d6eae64ed2bf20 5e30f2b1dd6e&ckck=1.

[25]   K. Yoshida, T Yokozeki. *Characterization of Interlaminar Fracture Toughness of CFRP Laminates Toughned by CNT-Dispersed Resin Interlayers.*

[26]   Ronald F. Gibson, Vijay Anumandla, Xin Wu. *Experimental Characterization of Delamination in Unidirectional Carbon/Epoxz Composite Specimens Featuring a Carbon Nanotube-Enhanced Ply Interface.* s.l. : Mechanical engineering department.

[27]   *Influence of fibre volume fraction on mode II interlaminar fracture toughness of glass/epoxy using the 4ENF specimen.* P. Davies, P. Casari, L.A. Carlsson. Florida Atlantic University : s.n., 2004.

[28]   Ki-Young Kim, Lin Ye, Kim-Meng Phoa. *Interlaminar Fracture Toughness of CF/PEI and GF/PEI Composites at Elevated Temperatures.* 2004.

8.2 List of variables and abbreviations

Abbreviation	Unit	Description
A	[m2]	Crack area
a	[m]	Crack length
a0	[m]	Initial crack length
ASTM	-	American Society for Testing and Materials
b	[m]	Width
BT	-	Beam theory
BUT	-	Brno University of Technology
Cs	[Pa m1/2]	Surface energy
C	[m Pa-1]	Compliance
CC	-	Compliance calibration
CFRP	-	Carbon fiber reinforced plastic
CNT	-	Carbon nanotubes
d11	[Pa m3]	Twisting bending matrix coefficient
DCB	-	Double cantilever beam
E	[Pa]	Young`s modulus
ENF	-	End notched flexure
G	[J m-2]	Energy strain release rate
Gc	[J m-2]	Critical strain release rate
Gic	[J m-2]	Critical strain release rate mode I
GiIc	[J m-2]	Critical strain release rate mode II
Gp	[J m-2]	Plastic energy dissipation
h	[m]	Height
H.O.T	-	High order terms
K	[Pa m1/2]	Stress intensity factor
Kic	[Pa m1/2]	Fracture toughness mode I
KIIc	[Pa m1/2]	Fracture toughness mode II
KIIIc	[Pa m1/2]	Fracture toughness mode III
l	[m]	Length
MBT	-	Modified beam theory
MCC	-	Modified compliance calibration
METU	-	Middle East Technical University
MWNT	-	Multi walled nanotubes
n	[-]	Correction factor - CC
Nc	[-]	Critical number of cycles
Nd	[-]	Detectable crack number of cycles
P	[N]	Force
R	[Pa]	Geometrical and material coefficient -CC
Rm	[Pa]	Ultimate strength
SF	[-]	Safety factor
SWNT	-	Single walled nanotubes

TAI	-	Turkish aerospace industry
tBI	[cycles]	Time between inspection
U	[J]	Elastic energy
UD	-	Unidirectional
α	[rad]	Correction factor - MCC
γ	[Pa m]	Surface energy density
σf	[Pa]	Fracture stress
Δ	[m]	Correction factor - MBT
δ	[m]	Displacement

8.3 List of figures

8.4 List of tables

8.5 List of appendixes

DCBDatabaseVUT+METU.xlsx
DCBscriptVUT_METU.m
ENFDatabaseVUT+METU.xls
ENFscriptVUT_METU.m